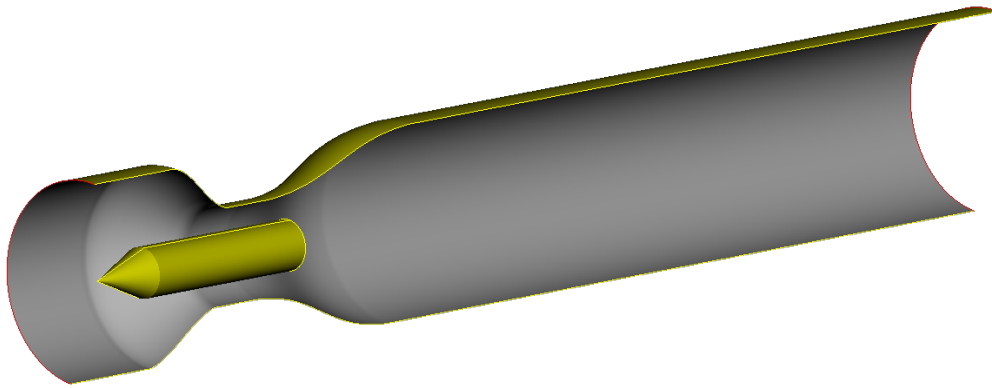




CHALMERS



Optimization and Automated Parameter Study for Cavitating Multiphase Flows in Venturi - CFD Analysis

Master's Thesis in Sustainable Energy Systems

KRISTIAN FRENANDER

Department of Applied Mechanics

Division of Fluid Dynamics

CHALMERS UNIVERSITY OF TECHNOLOGY

Gothenburg, Sweden 2014

Master's thesis 2014:61

MASTER'S THESIS IN SUSTAINABLE ENERGY SYSTEMS

Optimization and Automated Parameter Study for
Cavitating Multiphase Flows in Venturi - CFD Analysis

KRISTIAN FRENANDER

Department of Applied Mechanics
Division of Fluid Dynamics
CHALMERS UNIVERSITY OF TECHNOLOGY
Gothenburg, Sweden 2014

Optimization and Automated Parameter Study for Cavitating Multiphase Flows
in Venturi - CFD Analysis

KRISTIAN FRENANDER

©KRISTIAN FRENANDER, 2014

Master's Thesis 2014:61

ISSN 1652-8557

Department of Applied Mechanics

Division of Fluid Dynamics

Chalmers University of Technology

SE-412 96 Gothenburg

Sweden

Telephone +46 (0)31-772 1000

Cover:

3D representation of baseline case of venturi throat used for parameter study.

Chalmers Reproservice / Department of Applied Mechanics

Gothenburg, Sweden 2014

Abstract

In recent years falling demand for print paper and ambitious targets for reduction of energy use have been major factors that has caused the pulp and paper industry to develop state of the art technologies for reducing energy consumption drastically.

A method for achieving the same is to develop and design energy efficient refiners by utilizing hydrodynamic cavitation technology. A parameter study of a venturi design with a flow obstruction body is conducted in order to investigate the critical parameters for inducing hydrodynamic cavitation. To reduce computational time and thereby the costs, a second-level optimization algorithm using a Neural Network for a fixed set of samples is applied and investigated.

To create a real-life application for the design of venturi, outlet pressure, obstruction size and its position are found to be critical for maximizing cavitation zone in the centre axis of the flow field.

This research work does not consider fibres in the flow through the venturi.

The project has been conducted at ÅF Industry AB and is financed by Energimyndigheten, Stora Enso, Holmen, SCA and ÅF Industry AB

Key words: Multiphase flow, Optimization, Cavitation, Energy efficiency, Computational Fluid Dynamics, Artificial Neural Networks

Acknowledgements

This master's thesis is conducted as part the *Mekmassa project (E2MPi)* carried out by ÅF Industry AB in collaboration with Energimyndigheten, Luleå University of Technology, Stora Enso, SCA and Holmen. Advisors for the thesis are Vijay Shankar ÅF Industry AB, Lars Landström ÅF Infrastructure and Örjan Johansson at Luleå University of Technology. Examiner is Lars Davidson at Chalmers University of Technology.

I would like to thank all the people that have made this thesis possible, and especially my colleague Anton Lundberg for all his help and support and my supervisor Vijay Shankar for giving me the opportunity to do this, and helping me throughout the process. Thank you.

I would also like to thank my family for their continuous moral support and for giving me confidence and strength throughout this process, and all the friends that have given me good times and helped me keep my mind off cavitating flows every now and then.

And a special thanks to my girlfriend Johanna who has always been a massive support and inspiration for me. Thank you for putting up with me these years.

Kristian Frenander, Gothenburg, November 19, 2014

Contents

1	Introduction	1
1.1	Disc refiners	2
1.2	Proposed future design	4
2	Aim	5
2.1	Limitations	6
3	Theory	7
3.1	Fluid mechanics	7
3.1.1	Turbulence modelling	8
3.1.2	Multiphase flows	9
3.2	Cavitation	11
3.2.1	Bubble dynamics	12
3.3	Computer modelling	13
3.3.1	Mixture modelling	13
3.3.2	Bubble modelling	14
3.3.3	Cavitation modelling	14
3.4	Optimization	15
3.4.1	First level contra second level optimization	15
3.4.2	Multiobjective optimization	15
3.4.3	Latin Hypercube Sampling	16
3.4.4	Artificial Neural Network	17
3.4.5	Particle Swarm Optimization	18
4	Method	19
4.1	Calculations	19
4.1.1	Assumptions and simplifications	19
4.1.2	Mesh generation and morphing	20
4.1.3	Solver setup	21
4.2	Grid and iteration independence	23

4.2.1	Grid independence	23
4.2.2	Iteration and time-step independence	24
4.3	Parameter studies	26
4.3.1	Investigation number 1: Six parameters	27
4.3.2	Investigation number 2: Four parameters	28
4.3.3	Parameter sampling	29
4.3.4	Objectives for parameter study	30
4.3.5	Database generation	31
4.4	Optimization	31
4.4.1	Neural network	31
4.4.2	Optimization algorithm	32
5	Results	33
5.1	Investigation 1: Six parameters	33
5.1.1	Parameter influence	33
5.1.2	Pareto front	38
5.1.3	Geometry enhancement	39
5.1.4	Convergence study	41
5.2	Investigation 2: Four parameters	43
5.2.1	Parameter influence	43
5.2.2	Geometry enhancement	45
5.2.3	Convergence study	47
5.3	Summary	50
6	Discussion	51
6.1	Error margin	51
6.2	Source of errors	52
6.2.1	CFD simulations	52
6.2.2	Neural network solver approximation	53
6.2.3	Optimization	55
6.3	Accuracy of results	56
6.4	Simulation time consumption	56
6.5	Objective function	57
6.6	Optimal cases	57
7	Conclusion	59
8	Future work	61
8.1	Computer simulations	61
8.1.1	3D modelling	61
8.1.2	Modelling fibre flow	62
8.2	Experimental work	63
	Bibliography	67

1

Introduction

ENERGY CONSUMPTION has been rapidly increasing throughout the world since the onset of industrialization in the 18th century. As most of this energy has been produced using fossil fuels, the same has led to a rise in the concentration of CO₂ in the atmosphere to almost 400 ppm compared to a pre-industrial level of about 280 ppm, which is the highest level it has been at for 800 000 years (IPCC, 2013). This is a clear indication that human activities have severely altered the atmospheric composition and climate of our planet. Together with a broad range of events and environmental issues that have been highlighted since the 1960's this has instigated an awareness that measures must be taken to protect the environment if we are to sustain living conditions for both humans and other species on our planet. Selin (2014, chap 2) describes in brief the history of the environmental movement and the idea of sustainability.

To address the specific issue of climate change the European Union has adopted a set of objectives dubbed the *20-20-20-targets* for the year 2020 which are (European Commission, 2014):

- 20 % reduction of greenhouse gas emissions compared to 1990 levels.
- 20 % of the energy consumption should be produced from renewable sources
- 20 % improvement of the energy efficiency in the EU

Fulfilling these targets will be a considerable challenge for all member states, and in Sweden the government has proposed national targets in order to comply with the EU policy and a roadmap for a carbon neutral society in 2050. An important factor in achieving these targets is increased research and innovation efforts, with special focus on the heavy industry (Naturvårdsverket, 2012).

One of the industrial branches that is concerned is the pulp and paper industry, an

industry that consumes about 52 % of the energy consumed in the Swedish manufacturing sector on a yearly basis (Energimyndigheten, 2013). This makes it the individual sector with the largest energy consumption in Sweden's industry and a very relevant sector on which to focus research efforts on energy efficiency if targets of 20 % more efficient energy use by 2020 are to be met.

From a national Swedish perspective it is also interesting to reduce the energy consumption within the paper mills, as their production of energy from the biological residue of the pulping process is quite significant. In 2012 the energy production from bio-fuels in the Swedish pulp and paper industry amounted to 42.3 TWh (Statistiska centralbyrån, 2014). This means that if the energy consumption within the sector could be further reduced the paper mills could become net exporters of green bio-energy and thus contribute to a climate-neutral society.

The need is further amplified by the declining demand for newsprint paper putting financial stress on the industry. This means that the industry is hard pressed to cut costs, and given its large energy consumption, measures to reduce energy consumption could be crucial for keeping the Swedish pulp and paper industry sustainable in an ecological as well as an economical sense.

1.1 Disc refiners

When one analyzes the energy consumption in the production process, the disc refiners, where the wood chips are ground into fibres, stand out as a particularly energy demanding process step. With current techniques energy consumption can be up to several tens of megawatts for each disc refiner (Illikainen et al., 2007).

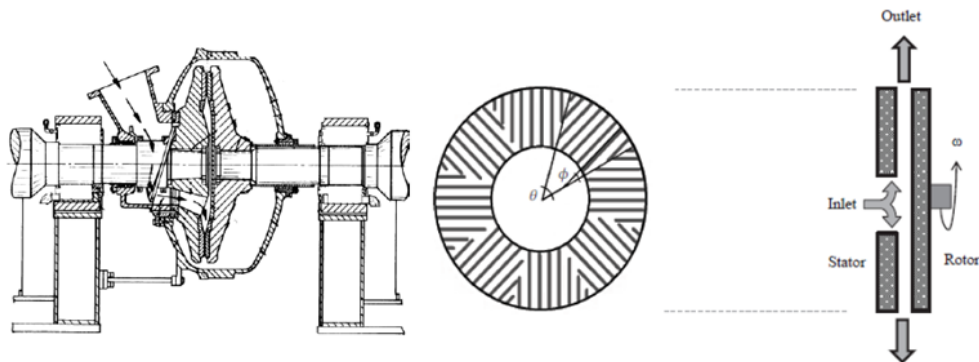


Figure 1.1: *Illustration of a disc refiner with axial inlet flow in the centre of the disc and radial outflow from the disc. On the left an entire overview can be seen, and on the right a closer view of the refiner plates, and patterns on the plate. Picture from Rajabi Nasab (2013).*

These refiners process the fibres mechanically with two or more rotating discs. These

rotating plates are patterned with slots and bars that at the same time force the fibres from the centre of the refiner to the periphery and grind the chips as they pass over them (Rajabi Nasab, 2013). This operation means that the fibres are processed using mechanical wear and friction which weaken the fibres and make the fibre walls collapse. However, research indicates that the passing of the slots over the fibres give rise to periodic pressure pulses in the ultrasonic range and cavitation (Eriksen and Hammar, 2007) that also contribute to the processing and fibrillation of the fibres (Gogate and Pandit, 2001). The cavitation is however undesirable despite its positive properties, as it also gives rise to significant mechanical wear and fatigue on the refiner plates because of the bubble collapses near the surface (Shankar, 2014).

The flow in the refiners pass from the inner part of the disc outward, as seen in Figure 1.1 where the larger radius of the disc is compensated by introducing more slots and bars on the disc. This means that the fibres need to pass over bars to fill the slots, which yields a rather complex flow pattern on the discs, and means that the frequencies of pressure fluctuation is different for different parts of the disc which influences the refinement of the fibres. An illustration of disc and fibre movement can be seen in Figure 1.2 which also illustrates gap clearance between plates.

In general two refiners are placed in series, with the first operating at higher fibre concentration and the second at lower concentration, or High Consistency (HC) and Low Consistency (LC) refiners. This means that the HC refiner breaks down wood chips to a more easily processed pulp which is mixed with extra water and refined further in the LC refiner. The HC refiner operates with a bigger gap clearance, i.e. distance between the two rotor discs, and the LC refiner has a smaller gap clearance which may be corresponding to only a few fibre diameters (Rajabi Nasab, 2013; Illikainen et al., 2007).

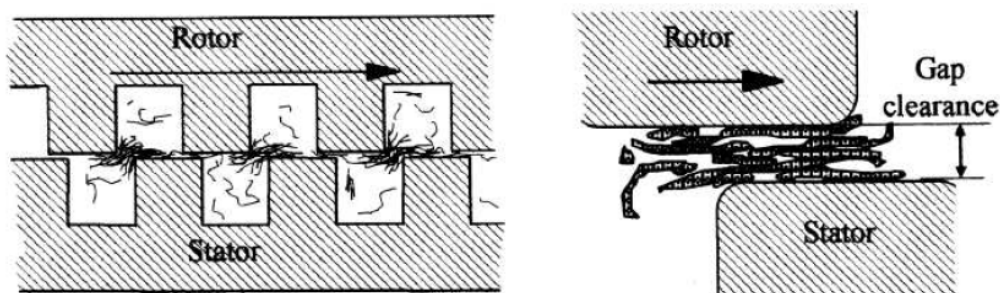


Figure 1.2: *Left: Illustration of flow between the plates in disc refiner. Right: Illustration of gap clearance between rotor and stator in refiner. Picture from Mroziński (2010).*

1.2 Proposed future design

An entirely novel technology for fibre refining has been suggested by Johansson and Landström (2010) with the purpose of significantly lowering the energy consumption in this step of the process. Their idea is based around cavitation, but instead of viewing it as an undesirable by-product that causes wear and fatigue on the machinery, they propose that the power of the bubble collapse should be utilized for the fibrillation and processing of the pulp fibres. The idea comes from the fact that cavitation has been noted to contribute to the fibrillation and processing of fibres already in the disc refiners in place today.

The design should induce hydrodynamic cavitation by running the pulp stream through a venturi nozzle. This is done to increase flow speed and reduce static pressure as both mass and energy must be conserved in the passage through the nozzle, for details see Section 3.2. The cavitation bubbles thus induced will then collapse when the pipe expands and the static pressure recovers, and the idea is to focus the bubble collapse on the surface of the fibres to achieve fibrillation and processing. This means that the venturi nozzle needs to be carefully designed so that the cavitation can be controlled and used to concentrate the processing energy to the fibres and provide effective refinement of the fibres in the flow. It might also be necessary to combine the hydrodynamic cavitation with acoustic control of the bubbles and the bubble collapse to achieve sufficient fibre processing. This would however require additional energy, so ideally the hydrodynamically induced cavitation will suffice for refining the fibres (Shankar, 2014).

The advantage with this technique compared with the current state-of-the-art is that it could possibly save large quantities of energy. This is due to a couple of beneficial aspects of cavitation. As cavitation can be created at near-ambient conditions regarding temperature and pressure it is a very energy efficient way of creating zones of high temperature and pressure gradients, namely the regions where the cavitation bubbles collapse (Gogate and Pandit, 2005). So instead of having to pressurize or heat the entire stream, similar effects can be achieved by inducing cavitation in the flow, where the only energy consumption correlates to the pressure drop over the cavitation zone. The most energy efficient manner to induce cavitation is by hydrodynamics, i.e. some sort of contraction-expansion vessel such as a venturi (Gogate and Pandit, 2001). This means that fluid-induced cavitation significantly reduces the amount of energy needed to create local zones of high temperature and pressure. The disadvantage is that it is hard to control and therefore has been considered too complicated to use on an industrial scale, but with the rapid development of CFD technology and engineering in the past decades the potential of hydrodynamic has received ever more interest, in particular from chemical and process industries (Gogate, 2011).

2

Aim

THE AIM of this project is to develop a new state-of-the-art technology for processing wood fibre and pulp using fluid induced hydrodynamic cavitation rather than mechanical processing as a mean to save energy in the pulp and paper sector.

As a first step to develop this technology a parameter study should be conducted on the venturi nozzle to find out which parameters are important for the amount of cavitation in the flow, and how an optimal venturi designed could be achieved. This is investigated by transient multiphase CFD simulations of cavitating flows, where the amount of cavitation in the system is measured.

The optimization is performed by implementing an advanced and efficient two level optimization scheme developed for single-phase flows and adapting it for multi-phase calculations. This requires a large number of simulations to be conducted. To be able to perform a sufficient amount of simulations they are conducted in an automated way by scripting both execution of CFD simulation and postprocessing of results.

The optimization seeks to satisfy multiple targets in both maximizing cavitation in the center of the stream after the venturi and simultaneously minimizing cavitation near the wall of the reactor. The maximization is defined some distance downstream the venturi to avoid direct bubble collapse and achieving a reasonable lifespan for the bubbles.

To summarize the aims are:

- Generalize and adapt an optimization method for multiphase flows.
- Perform a parameter study analyzing the influence on cavitation levels from geometric and pressure parameters.
- Increase knowledge of cavitation behaviour in a venturi with obstruction object.

2.1 Limitations

The study does not consider the size distribution and lifetime of the individual cavitation bubbles, nor does it specifically consider the mechanical damage that would be produced by bubble collapses near walls of the vessel. The mechanical wear is however considered when designing the objective functions for the optimization.

The energy consumption of the proposed design is not calculated at this stage. This is because the primary care is to obtain a workable design, and literature suggests it can safely be assumed to be less energy consuming than current devices.

The study does not consider fibres in the flow field in the venturi or how they would affect the formation of cavitation bubbles.

3

Theory

3.1 Fluid mechanics

FLUID MECHANICS is governed using a set of equations for conservation of momentum, energy and mass. These are the Navier-Stokes equation, energy conservation equation and the continuity equation. The Navier-Stokes equation for conservation of momentum can be written as follows using tensor notation according to Versteeg and Malalasekera (2007)

$$\frac{\partial \rho v_i}{\partial t} + \frac{\partial \rho v_j v_i}{\partial x_j} = -\frac{\partial p}{\partial x_i} + \mu \frac{\partial^2 v_i}{\partial x_j^2} + \rho g_i \quad (3.1)$$

where x_i denotes direction, v_i velocity in corresponding direction, ρ is the density and μ the dynamic viscosity. To clarify the tensor notation, this means for instance that when written out in the x-direction we obtain

$$\frac{\partial \rho u}{\partial t} + \frac{\partial \rho u u}{\partial x} + \frac{\partial \rho v u}{\partial y} + \frac{\partial \rho w u}{\partial z} = -\frac{\partial p}{\partial x} + \mu \left(\frac{\partial^2 u}{\partial x^2} + \frac{\partial^2 u}{\partial y^2} + \frac{\partial^2 u}{\partial z^2} \right) + \rho g_x \quad (3.2)$$

This is then reiterated for the other coordinate directions in the cartesian coordinates so that a complete formulation is obtained.

Using the same type of tensor notation the continuity equation can be written on a compact form as

$$\frac{\partial \rho}{\partial t} + \frac{\partial \rho v_i}{\partial x_i} = 0 \quad (3.3)$$

where ρ denotes density, t denotes time and v_i and x_i as above.

3.1.1 Turbulence modelling

Turbulent flows, which are the most common in everyday life, are characterized by irregularity, dissipation, large Reynolds number and threedimensionality. They may appear to be stochastic but are in fact governed by the Navier-Stokes equation 3.1. However, in order to fully calculate all turbulence effects on a flow would require it to be extremely well refined both in space and time, and for most problems this requires computational resources beyond what is actually available. To still be able to do good predictions using CFD turbulence can instead be modelled using one of several models available. In this particular case the emphasis will be put on the $k-\omega-SST$ -model.

$k-\omega-SST$ model

This model is a combination of the $k-\varepsilon$ and the $k-\omega$ model and was originally proposed by Wilcox in 1988 . The $k-\omega$ model in itself received a lot of attention as, in contrast with the commonly used $k-\varepsilon$ models, it does not require any near wall damping. ω is the turbulence frequency calculated as $\frac{\varepsilon}{k}$ with the dimension s^{-1} . This means the length scale can be calculated as $l = \sqrt{k}/\omega$ and eddy viscosity as $\mu_t = \rho k/\omega$.

As stated in Davidson (2014) $k-\varepsilon$ models have two notable weaknesses: overpredicting shear stresses in adverse pressure gradient flows and the need for near-wall modification. However as Menter (1992) noted, the $k-\omega$ model was more sensitive to assumed values in the free stream, which led to him proposing a hybrid model combining both $k-\varepsilon$ and $k-\omega$ as a way to benefit from the strengths of both models. Versteeg and Malalasekera (2007) formulate the governing equations for this model, where

$$\frac{\partial(\rho k)}{\partial t} + \text{div}(\rho k \mathbf{U}) = \text{div} \left[\left(\mu + \frac{\mu_t}{\sigma_k} \right) \text{grad}(k) \right] + P_k - \beta^* \rho k \omega \quad (3.4)$$

is the transport equation for k with

$$P_k = \left(2\mu_t S_{ij} - \frac{2}{3} \rho k \frac{\partial U_i}{\partial x_j} \delta_{ij} \right)$$

as the production rate of turbulent kinetic energy and

$$\begin{aligned} \frac{\partial(\rho \omega)}{\partial t} + \text{div}(\rho \omega \mathbf{U}) = & \text{div} \left[\left(\mu + \frac{\mu_t}{\sigma_{\omega,1}} \text{grad}(\omega) \right) \right] \\ & + \gamma_2 \left(2\rho S_{ij} \cdot S_{ij} - \frac{2}{3} \rho \omega \frac{\partial U_i}{\partial x_j} \delta_{ij} \right) - \beta \rho \omega^2 + 2 \frac{\rho}{\sigma_{\omega,2} \omega} \frac{\partial k}{\partial x_k} \frac{\partial \omega}{\partial x_k} \end{aligned} \quad (3.5)$$

is the transport equation for ω , which is obtained by substituting $\varepsilon = k\omega$ in the governing equation for ε in $k-\varepsilon$ model.

This model has subsequently been improved and in Versteeg and Malalasekera (2007) the major modifications are listed as

Table 3.1: Revised model constants for the $k - \omega - SST$ -model, as listed in Versteeg and Malalasekera (2007).

$\sigma_k = 1.0$	$\sigma_{\omega,1} = 2.0$	$\sigma_{\omega,2} = 1.17$	$\gamma_2 = 0.44$	$\beta_2 = 0.083$	$\beta^* = 0.09$
------------------	---------------------------	----------------------------	-------------------	-------------------	------------------

- Revising the model constants, as seen in Table 3.1.
- Blending functions used for the transition between the two models.
- Limiting the eddy viscosity for improved performance. Limiters are formulated as

$$\mu_t = \frac{a_1 \rho k}{\max(a_1 \omega, S F_2)}$$

with $S = \sqrt{2S_{ij}S_{ij}}$, $a_1 = \text{constant}$ and F_2 a blending function. And a second limiter

$$P_k = \min \left(10\beta^* \rho k \omega, 2\mu_t S_{ij} \cdot S_{ij} - \frac{2}{3} \rho k \frac{\partial U_i}{\partial x_j} \delta_{ij} \right)$$

3.1.2 Multiphase flows

Multiphase flows can be simply described as the simultaneous flow of two or more phases, which could be two phases of one species, e.g. water and steam, or multiple species, e.g. water and air. Characterization of multiphase flows is done according to the phases present and the four main cases are gas-liquid, gas-solid, liquid-solid and three-phase flows. Multiphase can also be categorized according to how the phases mix and form contact surfaces. These are defined by Crowe and Michaelides (2005) as:

- Dispersed flow is a flow where one phase is discrete elements in a continuous phase, such as droplets in gas flow or bubbles in liquid. In this case the discrete phases are not in contact with each other.
- Separated flow means the phases have only line of contact, for instance an annular ring of liquid on a pipe with gas flow in the centre.

Euler-Euler approach

In the Euler-Euler approach the different phases are treated as interpenetrating continua and combined using the concept of volume fraction, it ensures that the same volume cannot be occupied by multiple phases at once. The volume fraction function is assumed to be continuous in space and time and sum to one (ANSYS® Academic Research).

In a full Euler-Euler approach the phases are treated on their own with a set of governing equations solved for each phase individually and coupling between the phases is achieved by a shared pressure and common exchange coefficients between the phases (Crowe, 2005). For details on interaction and exchange between phases see section 3.2.

Mixture model

The mixture model is a somewhat simplified version of the full Euler-Euler approach where the fluid properties are calculated as mixture properties, for instance mixture velocity or mixture viscosity.

In the relevant case, where two fluids are modelled, the governing equations for the mixture model become (3.6) for continuity, (3.7) for momentum and (3.8) for energy, subscript m indicates mixture property.

$$\frac{\partial}{\partial t} (\rho_m) + \nabla \cdot (\rho_m \mathbf{U}_m) = 0 \quad (3.6)$$

is the continuity equation, where \mathbf{U}_m is the mass-averaged velocity and ρ_m is the mixture density, defined as $\rho_m = \sum_{k=1}^n a_k \rho_k$ where a_k is the volume fraction of phase k .

$$\begin{aligned} \frac{\partial}{\partial t} (\rho_m \mathbf{U}_m) + \nabla \cdot (\rho_m \mathbf{U}_m \mathbf{U}_m) = & -\nabla p + \nabla \cdot [\mu_m (\nabla \mathbf{U}_m + \mathbf{U}_m^T)] \\ & + \rho_m \mathbf{g} + \mathbf{F} + \nabla \cdot \left(\sum_{k=1}^n a_k \rho_k \mathbf{U}_{dr,k} \mathbf{U}_{dr,k} \right) \end{aligned} \quad (3.7)$$

is the momentum equation for the mixture model where μ_m is the viscosity of the mixture and $\mathbf{U}_{dr,k}$ is the drift velocity for the secondary phase $\mathbf{U}_{dr,k} = \mathbf{U}_k - \mathbf{U}_m$.

$$\frac{\partial}{\partial t} \sum_{k=1}^n (a_k \rho_k E_k) + \nabla \cdot \sum_{k=1}^n (a_k \mathbf{U}_k (\rho_k E_k + p)) = \nabla \cdot (k_{\text{eff}} \nabla T) + S_E \quad (3.8)$$

which is the energy equation with k_{eff} as the effective conductivity which is defined according to the turbulence model used, and S_E is a volumetric heat source.

By solving these equations for the mixture properties the flow is principally treated as a one-phase flow with the properties as a weighted mean value of the properties of the phases being modelled. To track the phases a transport equation for the volume fraction for the secondary phase is introduced and slip velocity between the phases is calculated. The volume fraction equation is formulated for phase p as

$$\frac{\partial}{\partial t} (a_p \rho_p) + \nabla \cdot (a_p \rho_p \mathbf{U}_m) = -\nabla \cdot (a_p \rho_p \mathbf{U}_{dr,p}) + \sum_{q=1}^n (\dot{m}_{qp} - \dot{m}_{pq}) \quad (3.9)$$

where \dot{m}_{qp} is the mass transport from phase q to phase p and \dot{m}_{pq} is the opposite mass transfer.

3.2 Cavitation

Cavitation is most easily described by using the Bernoulli equation for incompressible flow

$$p + \frac{1}{2}\rho v^2 = \text{const.} \quad (3.10)$$

where p denotes the local static pressure, ρ is the density of the fluid and v is the velocity of flow. According to this principle the static pressure must decrease when the flow velocity is increased. When the static pressure thus drops below the vapour pressure of the fluid it will lead to the formation of gas bubbles in the fluid flow, which is known as cavitation. This can be induced in flow by making the flow pass through a smaller pipe orifice which means that flow velocity must increase to satisfy continuity.

Cavitation is in many ways similar to boiling, see Figure 3.1, but not limited by the heat transfer in the liquid, rather only limited by inertial effects of the cavitating liquid. This means that cavitation is a much quicker process than boiling. The quick expansions and implosions of the bubbles is the reason it can be quite a damaging process. As the local pressure needs to be lower than the saturation pressure cavitation can occur once the cavitation number is lower than zero, see Equation 3.11. However, if one is able to predict where this can occur and control the cavitating flows, these violent processes could be put to good use (Gogate and Pandit, 2001). Several studies have also been conducted on the pressure development and erosion of collapsing cavitation bubbles and a number of them are reviewed in Okada et al. (1989). Though results vary somewhat between the studies the bubble collapse pressures are typically on the scale of thousands of megapascal.

Several studies have been conducted on how cavitation can be modelled, and which important parameters need to be fulfilled for cavitation to occur. The basic considerations are listed in Sauer (2000) where he for example states the basic cavitation number defined as

$$\sigma = \frac{p - p_{sat}}{\frac{1}{2}\rho_l U^2} \quad (3.11)$$

where p and p_{sat} are the static and saturation pressures, ρ_l is the liquid density and U is the liquid velocity. This is the dimensionless ratio of the pressure difference between static and saturation pressure and the dynamic pressure of the flowing liquid. However, in contrast to other dimensionless numbers cavitation can not be said to occur at one specific value, rather it depends on several mechanical and dynamic effects of the fluid, such as the number of cavitation nuclei, the friction and the surface tension (Sauer, 2000). Cavitation nuclei is considered as weak spots of the fluid structure and could for instance be solute gas, contact points with solid surfaces or small solid particles in the liquid.

The effects can be quite dramatic, for example theoretical work has found that a liquid free from nuclei could handle tension in the region of 1000 bar without breaking the liquid structure, while practical experience and experiments show that in general no

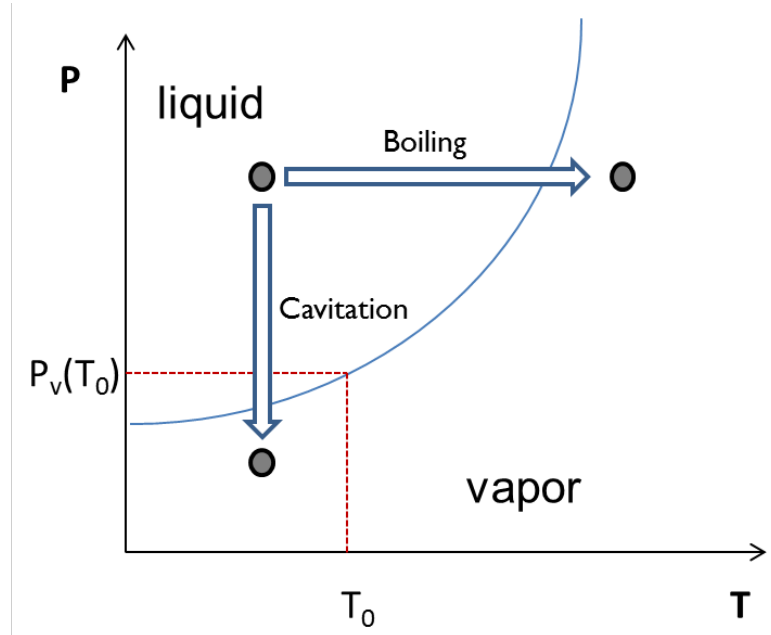


Figure 3.1: A phase diagram describing how cavitation occurs in a system by lowering pressure.

tension can be overcome (Sauer, 2000). Even under experimental conditions degassed and filtered water has not been able to withstand tensions larger than around 280 bar (Briggs, 1950). This can be explained by assuming that even very pure fluids have nuclei points and a pure fluid should be seen as an entirely theoretical concept. It also means that for engineering purposes it can usually be assumed that nuclei points are abundant and the fluid's ability to withstand tension is negligible.

3.2.1 Bubble dynamics

The dynamics of bubbles are described by the general Rayleigh-Plesset equation which is stated in Franc (2006) as

$$\rho \left[R\ddot{R} + \frac{3}{2}\dot{R}^2 \right] = [p_v - p_\infty(t)] + p_{g0} \left[\frac{R_0}{R} \right]^{3\gamma} - \frac{2S}{R} - 4\mu \frac{\dot{R}}{R} \quad (3.12)$$

where R denotes the bubble radius and \dot{R} and \ddot{R} are the first and second order time derivatives of bubble radius respectively. The surface tension is denoted as S and p_v and $p_\infty(t)$ are vapour pressure and the farfield pressure of the surrounding liquid respectively. This gives us a relation between the surrounding pressure and the temporal development of the bubble radius. It can clearly be seen that bubble radius will decrease with increasing liquid pressure, which means that cavitation bubbles will have a shorter

lifespan if the pressure recovery is quick after the orifice, and vice versa. The nonlinearities in Equation (3.12) however means that this is only a simplified way of looking at it, and that the response of bubbles subjected to changing pressures will be nonlinear. This contributes to the very drastic features of cavitation bubbles. For instance a drop in pressure leading to nonlinear increase in bubble radius implies a depressed vapour pressure inside the rapidly expanding bubble (Crowe et al., 2011). This low pressure inside the bubble can further amplify the rapid collapse due to very high pressure gradients over the bubble wall.

It is important to note that the Rayleigh-Plesset equation has been derived for adiabatic conditions for the control volume surrounding the bubble, as the evolution of the bubble is so quick that the heat transfer will be negligible for these time scales. This means that conditions in the control volume will not be isothermal and the heat needed for vapourization will be provided by a volume of the liquid surrounding the bubble. Due to this both temperature and pressure will vary quite heavily on very small scales (Franc and Michel, 2006).

3.3 Computer modelling

In order to implement the physical models computationally some simplifications are made to reduce the computational effort.

3.3.1 Mixture modelling

In order to allow for different velocities of the different phases slip velocity need to be introduced and is defined as

$$\mathbf{v}_{pq} = \mathbf{v}_p - \mathbf{v}_q \quad (3.13)$$

However the individual velocities are unknown, so the slip velocity is calculated using an algebraic formulation in the FLUENT[®] implementation of the mixture model (ANSYS[®] Academic Research). This is done by assuming that local equilibrium is reached over short length scale and is defined as

$$\mathbf{v}_{pq} = \frac{\tau_p}{f_{\text{drag}}} \frac{(\rho_p - \rho_m)}{\rho_p} \mathbf{a} \quad (3.14)$$

where τ_p is the particle relaxation time

$$\tau_p = \frac{\rho_p d_p^2}{18\mu_q}$$

d_p is the diameter of particles of the secondary phase and \mathbf{a} is acceleration of the secondary phase computed as

$$\mathbf{a} = \mathbf{g} - (\mathbf{v}_m \cdot \nabla) \mathbf{v}_m - \frac{\partial \mathbf{v}_m}{\partial t}$$

3.3.2 Bubble modelling

Modelling cavitating flows is a computationally expensive procedure, so in order to reduce the calculations some simplifications are done when computing bubble size in the standard FLUENT cavitation model (ANSYS® Academic Research). In Equation (3.12) second-order terms are neglected along with surface tension force yielding the simplified form

$$\dot{R} = \sqrt{\frac{2}{3} \frac{p_v - p_\infty}{\rho_l}} \quad (3.15)$$

which significantly reduces computational effort for bubble dynamics.

3.3.3 Cavitation modelling

The Schnerr and Sauer model implemented is based on the model they proposed in (Schnerr and Sauer, 2001). The equation governing the vapour volume fraction is then formulated as

$$\frac{\partial}{\partial t} (a\rho_v) + \nabla (a\rho_v \mathbf{U}_v) = \frac{\rho_v \rho_l}{\rho} \frac{Da}{Dt} \quad (3.16)$$

where index v indicates vapour property and index l indicates liquid property.

The mass transfer rate is then the mass source term modelled as

$$\mathfrak{R} = \frac{\rho_v \rho_l}{\rho} \frac{da}{dt} \quad (3.17)$$

from the right hand side of Equation (3.16).

This is complemented with a model for the connection between volume fraction and number of bubbles per liquid volume used to refine the source term describing the mass flow between the two phases

$$a = \frac{n_b \frac{4}{3} \pi R_B^3}{1 + n_b \frac{4}{3} \pi R_B^3} \quad (3.18)$$

which is used to obtain a refined equation for mass transfer defined as

$$\mathfrak{R} = \frac{\rho_v \rho_l}{\rho} a(1-a) \frac{3}{R_B} \sqrt{\frac{2}{3} \frac{(P_v - P)}{\rho_l}} \quad (3.19)$$

where the bubble radius is calculated as

$$R_B = \left(\frac{a}{1-a} \frac{3}{4\pi n} \right)^{1/3} \quad (3.20)$$

3.4 Optimization

The optimization algorithm implemented is based on the method developed in (Lundberg, 2014) and for a more detailed explanation the reader is referred to this thesis. Only a brief summary of the underlying theory is presented in this section.

3.4.1 First level contra second level optimization

Classical optimization algorithms have used the straightforward approach of conducting the optimization directly on the experiment or solver. This means the the calculation is run for every iteration and the model is updated according to some optimization goal for each iteration until sufficient convergence is reached, see Figure 3.2 for method schematic.

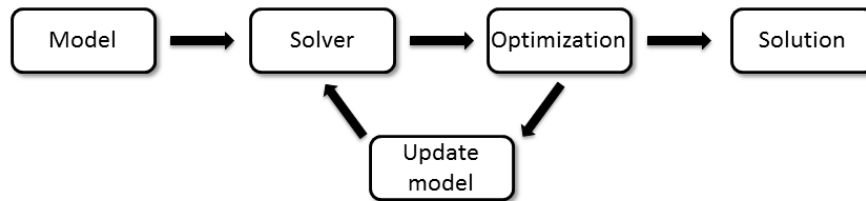


Figure 3.2: A schematic representation of first level optimization with direct solver looping. With kind permission from Lundberg (2014).

Second level optimization instead uses a predefined sample space, see section 3.4.3, to create a set of configurations that need to be computed. Using the output database from these experiments a solver approximation can then be created, in form of a response surface or, as in this case, an Artificial Neural Network, see section 3.4.4. The solver approximation can be seen as a representation of a much larger set of configurations on which the optimization then can be run, see Figure 3.3 for a schematic of the method. This means that the optimization can be done in a much quicker way than would be possible if each configuration had to be simulated computationally. This allows for many different optimizations to be done and optimization targets to be altered with minimal effort.

3.4.2 Multiobjective optimization

Optimization with multiple objectives means a possible trade-off where one objective may be improved at the expense of another objective. To account for this in optimization terms the *Pareto Front* is introduced. It can be understood as the set of points where no improvement can be achieved in one objective without worsening another objective.

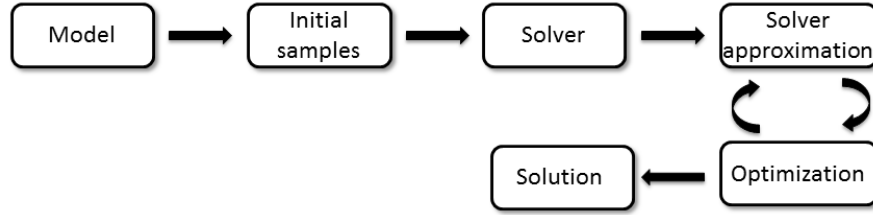


Figure 3.3: Schematic representation of second level optimization where optimization iterations are performed on an approximation of the solution to minimize the need of costly computations. With kind permission from Lundberg (2014).

Lundberg (2014) formulates this as:

A tensor \mathbf{u} dominates \mathbf{v} where $(\mathbf{u}, \mathbf{v} \in \mathcal{R}^k)$ if

$$\mathbf{u} \neq \mathbf{v} \text{ and } u_i \leq v_i \forall i \quad (3.21)$$

and a point $\mathbf{x} \in \mathcal{R}^k$ with the objective function $\mathbf{f}(\mathbf{x})$ is nondominated if

$$\nexists \mathbf{x}' \in \mathcal{R}^k \text{ such that } \mathbf{f}(\mathbf{x}') \text{ dominates } \mathbf{f}(\mathbf{x}) \quad (3.22)$$

where a point is called Pareto optimal if it is nondominated on the search domain.

3.4.3 Latin Hypercube Sampling

Sampling is used to determine which configurations should be simulated to construct the database that is used for the solver approximation. In order to minimize computation time the parameters must be sampled in a way that allows broadest possible span of the parameters to be examined using minimum amount of computations. One such method is the Latin Hypercube Sampling (LHS), here presented in two dimensions. The sample space is divided into a number of rows and columns and the space is sampled once for each row and column, so for instance a case with four rows and four columns would be sampled four times, as seen in Figure 3.4.

This method has a smaller variance than random sampling while allowing for fewer samples than a full-factorial design (Fang et al., 2006), which is an important factor for reducing costly computations. A weakness of LHS is however that it does not reach minimal variance, i.e. it risks picking points that are quite close to each other despite being in different rows and columns. This weakness is compensated for by running a Monte Carlo simulation on top of the LHS generation. This means that a large number of LHS designs are generated and the minimum distance between sampling points is calculated. The case with the largest minimum distance is then chosen as the base for the optimization.

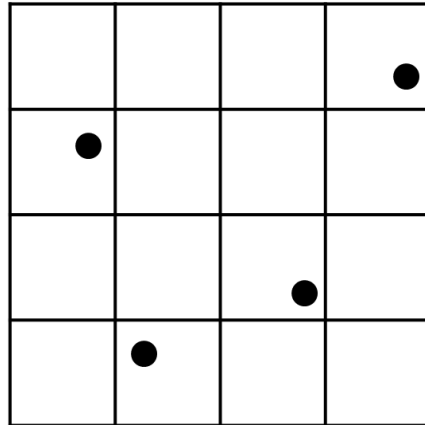


Figure 3.4: An example of 2D LHS sampling with four samples, i.e. two per parameter. With kind permission from (Lundberg, 2014).

3.4.4 Artificial Neural Network

The solver approximations is used to create an approximate of the solution for configurations that have not been simulated. The optimization can then be conducted on the solver approximation.

The solver approximation was obtained by implementing an artificial neural network that seeks to mimic the function of an organic nervous system by replacing the neurons with computational nodes that are trained with the results obtained from the solver. This method is very good at capturing non-linear behaviour in the data which is important to be able to capture when optimizing a complex problem where the results are hard to predict.

To train the neural network input data is transferred through the network with a fixed set of weights and then compared to the output data. Using the error that occurs the weights are then adjusted and the information is instead fed back through the network to adjust to the data. This process is called *back-propagation method* (Van den Braembussche, 2008). By repeating this process the neural network can learn to mimic the behaviour of the system being researched.

Overtraining

A danger when training the network is to overtrain the network, which is when the database used for training is too big and causes the network to adapt to closely and mimic also non-general behaviours of the input data, such as noise.

Regularization

Regularization assumes that the function being approximated is smooth, meaning that there are no discontinuities in the system. To obtain a smooth response from the neural network the weights need to be kept small and simultaneously minimize both the sum of square of the weights, E_W , and the sum of squared output error, E_T . Foresee and Hagan (1997) state this minimization problem as

$$E = \alpha E_T + \beta E_W \quad (3.23)$$

where the main task is to find the optimal values for α and β . Foresee and Hagan (1997) propose a generalizable method for doing this that has been implemented in MATLAB function *trainbr*.

3.4.5 Particle Swarm Optimization

PSO is an evolutionary optimization algorithm first suggested by Eberhart and Kennedy (1995) that combines local and global optimum search. This is done in a way that mimics how a flock of birds searches for food. The individuals are spread out over a search area, corresponding to the sample size of parameters, and each individual performs a local search whilst communicating with the rest of the flock to yield a simultaneous global search. This method is very robust, and the random element of the search and continuous search over a large part of the domain makes it less likely to get stuck at local optima.

4

Method

EXTENSIVE PARAMETER STUDIES were conducted to identify relevant and critical parameters with respect to design of venturi. The same was achieved by varying a large set of parameters. Below is a detailed description of the method and tools employed during the investigations.

4.1 Calculations

All calculations were carried out using commercial CFD software FLUENT in combination with mesh generation program ANSA and post processing program MATLAB.

4.1.1 Assumptions and simplifications

Modelling hydrodynamic cavitation and bubble growth and its collapse is highly complicated and time consuming. Simulations costs are high. It is therefore important to apply sensible assumptions and modifications in order to minimize the computational resources needed to solve the problem on hand. This becomes even more important when one needs to simulate a large number of cases and at the same time investigate the influence of several parameters.

- All simulations were conducted as two-dimensional axisymmetric.
- Abundant cavitation nuclei exist in the fluid for all time-steps.

Assumptions increase the risk of deviance between real solution and simulation, so it is important to note this when analyzing the results. It is however necessary to investigate many different parameters that influence the flow field.

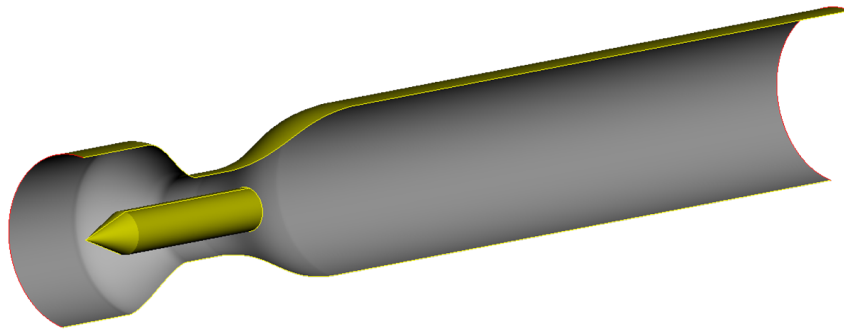


Figure 4.1: *The general concept studied, a venturi pipe with a centred flow obstruction. The pipe is designed to be standing up, with gravity working in the flow direction.*

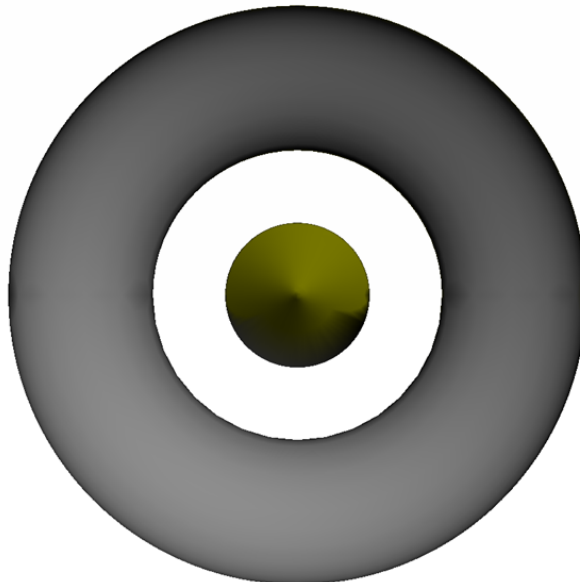


Figure 4.2: *The baseline configuration of the venturi as seen from the perspective of incoming flow.*

4.1.2 Mesh generation and morphing

All meshes were generated in ANSA using a baseline case drawn up manually, which was then morphed using the DFM-tool operating on the curves defining the basic geometry. Once this morphing was conducted a face was created using the curves, and mesh numbering parameters were set according to values obtained from the mesh independence analysis, see Section 4.2. A quad-mesh was then generated using the *Gradual* method in ANSA. The mesh for the baseline case can be seen in Figure 4.3 and an example of a mesh in a morphed case can be seen in Figure 4.4.

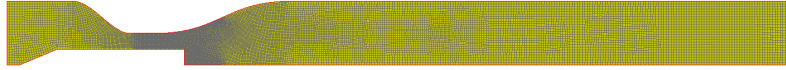


Figure 4.3: *The auto-generated mesh for the baseline configuration.*



Figure 4.4: *An example of a mesh for an arbitrary morphed configuration.*

4.1.3 Solver setup

The solver used is a pressure-based Navier-Stokes solver with $k-\omega$ SST turbulence model. The multiphase calculations utilizes the mixture model presented in Section 3.1.2 and cavitation is modelled with the Schnerr and Sauer model assuming abundant presence of nuclei for bubble formation.

Schnerr and Sauer is the default cavitation model in FLUENT. It is chosen for stability and speed of convergence.

Multiphase calculation, especially cavitating flows, are inherently unstable and difficult to obtain a converged solution and therefore need to be fine-tuned. By activating different models gradually, the case was allowed to converge to a reasonable level for every model implemented in that stage, before adding another level of complexity to the calculations. The basic process is explained in Figure 4.5. A summary of the steps are

- Read case mesh and set boundary conditions
- Initiate flow by conducting 500 iterations with first order discretization
- Turn on higher order discretization and perform 500 more iterations
- Activate mixture model with Schnerr-Sauer cavitation model
- Perform 10 000 pseudo-transient iterations with user-defined length-scale of 5 mm
- Switch to transient simulations and perform 20 time-steps with 50 iterations per

time-step and time-step size $10 \mu\text{s}$

- Initialize transient flow with a further 1500 time-steps with 30 iterations per time-step and time-step size $50 \mu\text{s}$
- Start writing output data, exporting pressure, velocity, temperature and vapour fraction data every 10 time-steps
- Perform a further 4500 time-steps of size $50 \mu\text{s}$ while exporting data
- Exit simulation

This was done to make sure that the case was stabilized and converged before the output data was written as a way to avoid error in the results. The exact numbers of iterations and time-steps were found through an extensive iteration independence study, see section 4.2.

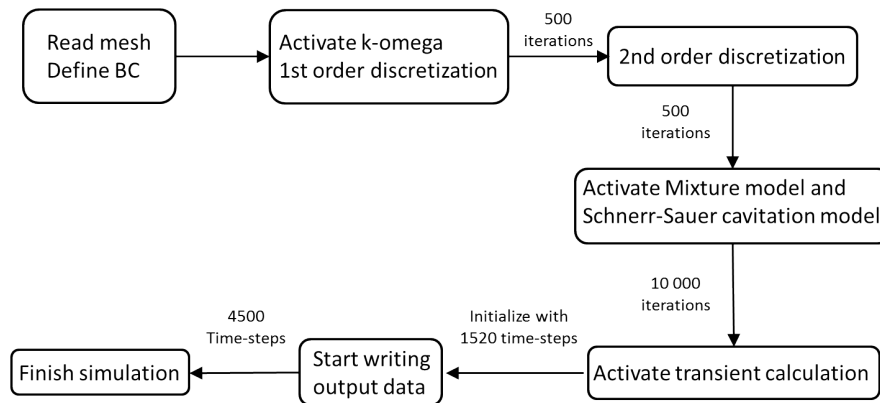


Figure 4.5: Flowchart showing how the simulations are conducted for each mesh.

Table 4.1: The boundary conditions set for the FLUENT 2D cases. Pressures were varied as part of parameter study, for specific values see tables 4.2 and 4.3.

ID	Boundary Condition
Inlet	Pressure Inlet
Outlet	Pressure Outlet
Axis	Symmetry Axis
Obstruction	Wall
Wall	Wall

4.2 Grid and iteration independence

When performing CFD analysis, it is important to make sure that the results reflect the physical characteristics of the flow field and are not the effect of numerical abnormalities. This can be achieved by investigating whether the case converges to the same solution independently of the calculation grid, or mesh, used for the simulation. In the studied case, the multiphase flow requires the grid to be finely refined to correctly capture the physical behaviour of the cavitating flow. How fine the resolution must be, is determined by performing a mesh analysis to find out the maximal allowed element size that yields constant results for a sufficient amount of iterations. The amount of iterations needed must also be analyzed to avoid either performing too many computations or obtaining a solution that is not sufficiently converged.

Besides the mesh, when performing transient simulations one must also analyze the amount of time-steps needed to initiate a solution that is either time-independent or periodically varying with time. To analyze this an identical case regarding geometry and boundary conditions is simulated for different meshes, amount of time-steps and iterations. Measurements were made for pressure, velocity and temperature along lines intersecting the pipe, see Figure 4.6. vapour fraction was also measured, but for five larger zones of the pipe in order to compensate for the unstable and fluctuating nature of the cavitation bubbles. This was done because the fluctuating and random nature of the vapour fraction in the pipe meant it needed to be measured over larger areas to capture its behaviour and correctly assess the model.

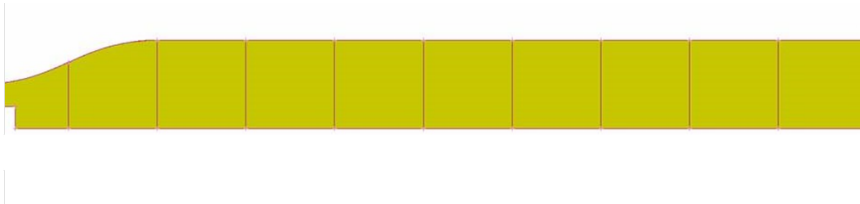


Figure 4.6: 2D model of the channel downstream the venturi with the lines where data is output from FLUENT marked.

4.2.1 Grid independence

To investigate the number of mesh elements needed to obtain a stable solution three different meshes of the baseline case were created using the *Gradual* meshing method provided in ANSA. The size of the meshes tested ranged from circa 1000 cells for the smallest mesh to 48000 cells for the largest mesh with the middle size containing circa 13000 cells. Simulations with the same settings were then conducted for all three meshes, with inlet pressure of 2 bar and outlet pressure of 1 bar. Measurements were made along the lines shown in Figure 4.6 for pressure, temperature and velocity. Apart from this,

the volume fraction was also measured for the entire geometry and averaged over five zones, defined equidistantly from the end of the obstruction to the outlet.

To analyze which grid resolution would be sufficient, output data from the three different meshes were compared, an example can be seen in Figure 4.7 where the average vapour fraction in the five zones are plotted for three different meshes. From this plot one can conclude that all cases have yielded the same type of trends, but the smallest mesh with only a thousand cells is consistently underestimating the amount of vapour in the system. In Figure 4.8 one can note that the two finer meshes correlate fairly well, where as the coarse mesh cannot fully capture the velocity profile of the flow, especially in the region near the wall.

Based on the results obtained from the simulations it was decided that the mesh with 13000 cells would be used for the parameter study. It captures the behaviour of flow sufficiently well, while still allowing for a large number of cases to be studied in a reasonable amount of time.

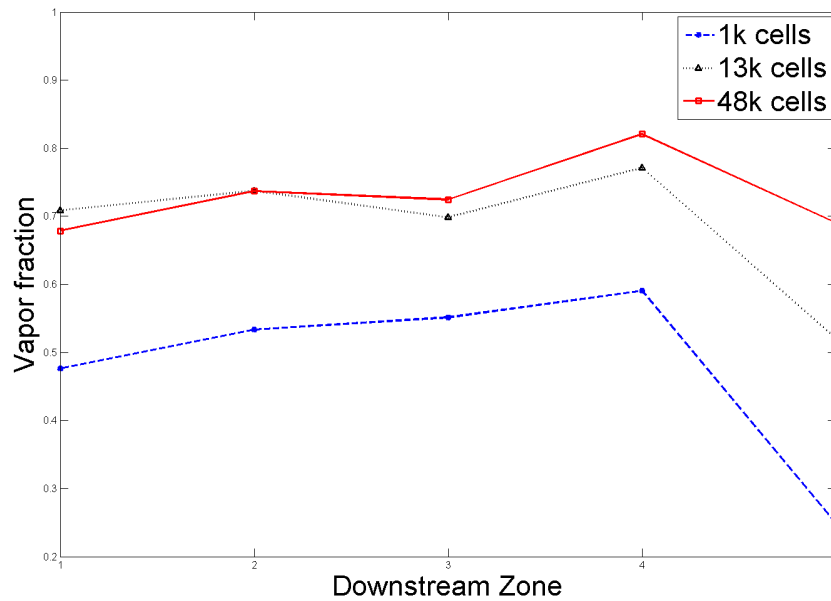


Figure 4.7: Average of vapour fraction in five zones downstream the venturi plotted for three different meshes. One can note that the 13k and 48k cases correlate fairly well, whereas the 1k case differs significantly.

4.2.2 Iteration and time-step independence

As a satisfactorily converged steady-state solution was unattainable for the case the results needed to be calculated as averages over many transient simulations instead.

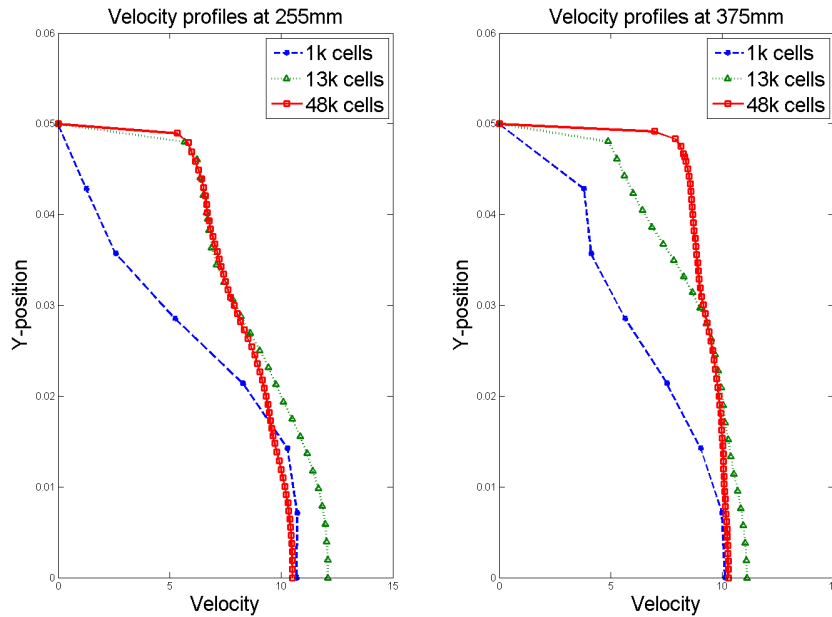


Figure 4.8: Velocity profile in the pipe measured at two different cross-sections in the pipe for the three different meshes.

When one conducts an investigation like this it is important to analyze how the flow develops over time, if it for instance stabilizes or is oscillating. If the flow oscillates it is important to measure over a couple of flow cycles.

It is also important to make sure that the time-step is small enough for the development of flow to be captured. However it cannot be too small as this means that too much computational effort is needed to simulate any substantial time-scales. For the relevant case this was determined by analyzing the cell sizes in the highly resolved regions of the flow and choosing a time-step so that flow particles do not travel a distance greater than one cell size during one time-step. This is the same as setting the Courant number to 1 or $\frac{u\Delta t}{\Delta x} = 1$. To calculate the time-step this yields $\Delta t = \frac{\Delta x}{u}$. As the resolution is the finest in the throat region of the venturi, where flow velocity is at its maximum, only this region is considered to be limiting the time-step. For the mesh with 13000 cells the smallest cell length is 0.5 mm and the maximum speed is about 20 m/s, meaning that the time becomes $\frac{0.0005\text{ m}}{20\text{ m/s}} = 2.5 \cdot 10^{-5}\text{ s}$ or 25 μs . The maximum velocity was calculated from test simulations where inlet pressure was 3 bar. A slightly higher Courant number can be accepted without divergence and deteriorating results, so in order to save computations the time-step was set to a maximum of 50 μs after the flow had been initialized.

This short time-step means that a large number of steps must be calculated in order to properly describe behaviour on larger timescales. To find the number of steps needed a test case was run over 4000 time-steps. In analyzing these results it was found that

after about 3500 time-steps the solution was stable with regard to larger averages of vapour fraction, though still oscillating locally, much of it due to eddies propagating down through the flow mixing gas and liquid parts of the flow. See Figure 4.9 for comparison between two time-steps after 3500 time-steps had been simulated. As the flow patterns can vary significantly between different configurations it was decided that all measurements should be averaged over 4500 time-steps after being initiated with a steady state solution and then 1500 transient time-steps.

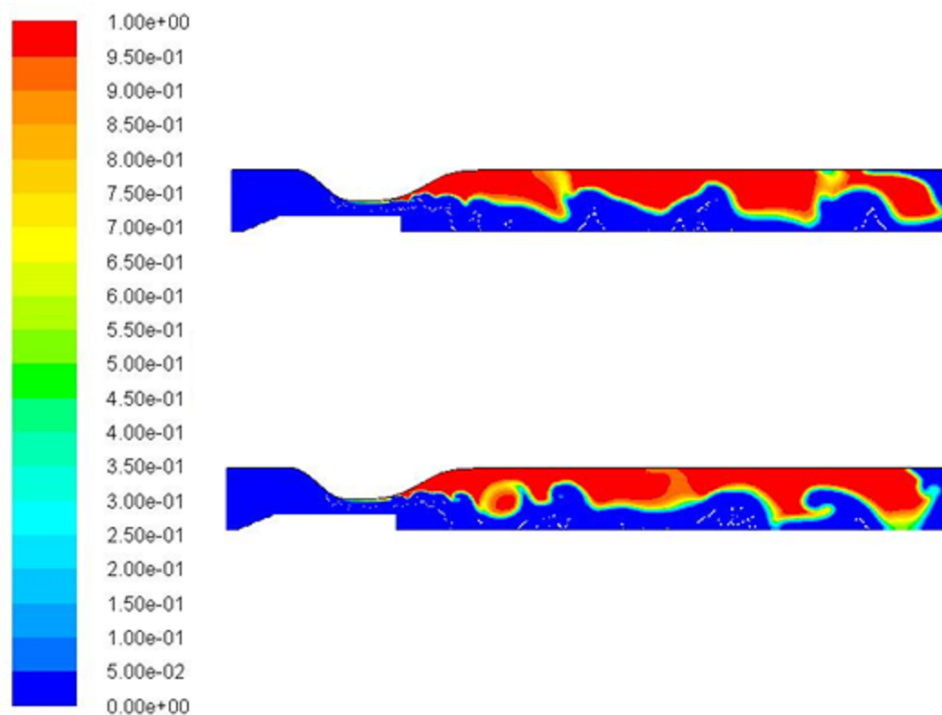


Figure 4.9: A comparison of volume fraction plots for two different time-steps with a common scale for volume fraction. The principal shape of both liquid and gas flow remains, with local fluctuations due to travelling eddies in the flow. The top sample is taken after 3535 time-steps, and the bottom one after 3975 time-steps.

4.3 Parameter studies

The study was split into two major investigations. The results from the first investigation was taken as input to the second in order to narrow down the scope of the second investigation.

4.3.1 Investigation number 1: Six parameters

The first substudy was done with a broader scope and included the six parameters listed in Table 4.2. In line with practice for training neural networks implemented by Lundberg (2014) 2⁶ or 64 different configurations were studied. On top of these a simulation was also run for the unmorphed baseline case, making it 65 simulations in total.

The parameters studied are mainly geometrical, concerning the shape of the venturi, and the shape and size of expansion and inlet zone. On top of this both inlet and outlet pressure were varied to find optimal values. The baseline concept investigated is shown in Figure 4.1 as seen from the side and in Figure 4.2 as seen from the perspective of incoming fluid.

In order to find out what influences the results, i.e. the amount of cavitation bubbles in the mid-stream zone after the venturi, a set of parameters was defined and the geometric parameters can be seen in Figure 4.10.

Obstruction ratio

This parameter, defined from $\frac{r_o}{r_t}$ in Figure 4.10, is the ratio between the obstruction object and the venturi throat. This is important as it determines the area of free passage that the flow is pushed through by the inlet pressure. In order to fulfill the continuity equation this parameter, together with *throat radius*, regulates the flow velocity through the venturi throat for the corresponding inlet pressure. It is defined as a ratio to throat radius to avoid filling the throat entirely, or creating cases where the obstruction is larger than the venturi. Therefore its limits are defined as percentages of the throat radius, see Table 4.2.

Curvature length

The curvature length, L_c in Figure 4.10, determines how sharp the expansion will be after the venturi throat. This is relevant as it determines whether the flow out of the throat will be attached or separated, which will have a big impact on the flow patterns downstream the venturi. It can be increased to smoothen the expansion, or decreased to make the expansion more rapid.

Obstruction length

The length of the flow obstruction object, L_o in Figure 4.10, is varied to investigate how the flow pattern is affected by the where the sudden expansion occurs. It morphs in both positive and negative x-direction.

Table 4.2: The parameters studied in the first parameter study and the range within which they were varied. Note that throat radius only scales downward, making the free passage smaller. All geometric values are normalised with inlet radius due to confidentiality.

Parameter	Lower Bound	Baseline	Upper Bound
Curvature Length	0.8	2	4
Obstruction Length	1.6	2	4
Obstruction Ratio	18 %	50 %	80 %
Throat Radius	0.3	0.5	0.5
Inlet Pressure	1.5 bar	2 bar	5 bar
Outlet Pressure	0.5 bar	1 bar	1.25 bar

Throat radius

The throat radius, r_t in Figure 4.10, is an important parameter in determining how much the flow should be accelerated in comparison with the inlet velocity, as the inlet radius is kept constant. Important to note is that the obstruction scales with the same percentage as the radius in order to avoid completely filling the venturi throat.

Inlet pressure

Inlet pressure is varied as it is an important factor in determining the flow velocity through the venturi throat. By examining the Bernoulli equation one realises that this is important for the static pressure in the venturi throat region.

Outlet pressure

Outlet pressure influences how quickly the pressure recovers after the venturi throat and acceleration. It is varied in order to see how this affects the size of the mid-stream cavitation zone downstream the venturi.

4.3.2 Investigation number 2: Four parameters

The first substudy indicated that curvature length had little, or quite unclear, impact on the objective function, see Chapter 5, and was fixed at the baseline value. It was also realized that throat radius and obstruction ratio could essentially be combined into one parameter denoted *obstruction radius* which is only the height of the obstruction object, the radius of the throat is fixed. Obstruction length was also somewhat redefined based on the wish to try a possible tuning parameter defined as *obstruction position*. This is

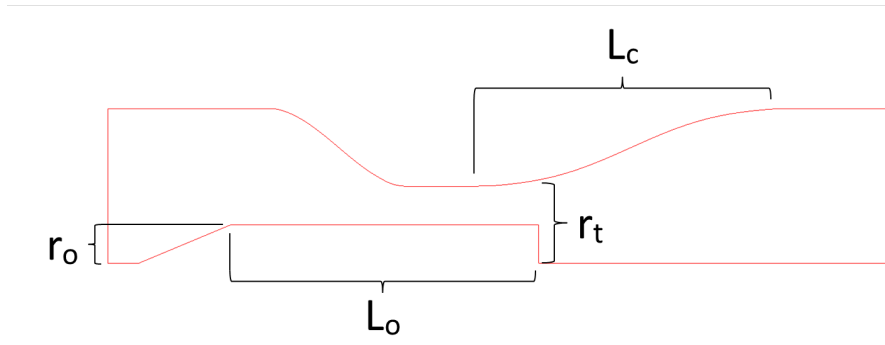


Figure 4.10: *The four geometry parameters defined for the study.*

defined as the distance from the inlet to the tip of the obstruction, with the size being kept constant. This is interesting due to the need for a control parameter that can be variable in the actual industrial application, which could be the obstruction position.

The studied span for both inlet and outlet pressure were raised in the second investigation. This was done to ensure both that the bubbles collapse at a higher surrounding pressure and to avoid that the entire flow cavitates downstream the venturi, see for instance Figure 5.7.

Thus for the second investigation, the following four parameters are studied:

- Obstruction radius
- Obstruction position
- Inlet pressure
- Outlet pressure

2^4 or 16 different sample configurations were tested apart from the baseline case, making it 17 simulations in total. This allowed for a larger number of time-steps to be simulated, raising the total number of time-steps from 6020 to 10020. This further ensures the system is properly initialized before any results are printed from the simulation. Other than this simulations are conducted in the same way as for substudy number 1.

4.3.3 Parameter sampling

To improve the accuracy of optimization utilizing artificial neural networks Van den Braembussche (2008) found that it is important to sample the parameters systematically rather than at random. To complement this Alam et al. (2004) compared different sampling methods and found that latin hypercube sampling, see Section 3.4.3, outperformed the other sampling algorithms tested. This is implemented in both substudies

Table 4.3: *The parameters and respective sampling range in substudy number two. All geometric values normalised with inlet radius due to confidentiality*

Parameter	Lower Bound	Baseline	Upper Bound
Obstruction Position	0.1	0.2	0.6
Obstruction Radius	0.1	0.25	0.4
Inlet Pressure	3 bar	3 bar	5 bar
Outlet Pressure	1 bar	1 bar	2.5 bar

to create the design samples to be simulated when building the database used for simulation.

4.3.4 Objectives for parameter study

As stated already in Chapter 2 the investigation seeks to maximize the cavitation in the centre of the pipe and minimize the cavitation near the wall. To perform this an objective function must be defined. But measuring cavitation in itself is not possible, so the objective must be defined differently. Noting that the inlet stream is pure liquid water, that then cavitates and forms vapour in the nozzle, the vapour fraction of the flow is chosen as the measurement for the objective function. But as noted in Section 4.2 the vapour fraction fluctuates over time and to avoid this disturbing the results the objective function needs to be defined as an average over time and over a fairly large number of nodes. The area can be seen in Figure 4.11 and an argument regarding the number of time-steps measured can be found in Section 4.2.

The measured vapour fraction is saved every ten time-steps of the calculation for the entire geometry, so in order to for the relevant data to be sampled it must be sorted by position in the mesh. This is done in the post-processing script in MATLAB where data is sampled after the flow is deemed sufficiently initialized. The data is measured for each computational cell, so in order to calculate a correct average the value is weighted with the size of the relevant cell to return an average for the entire zone for that time-step. The measurements from the different time-steps are then averaged to retrieve concise output data from each simulation. The zone is placed some distance from the venturi to ensure that the bubbles don't collapse instantly. The zone does not stretch all the way down to the outlet to avoid the outlet pressure having too big an impact on the measured results. The height is chosen to be half of the channel height, to avoid maximizing cavitation too close to the wall.

On top of this a second objective is defined for minimizing near-wall cavitation. The vapour fraction is measured along the wall, the entire way from the venturi throat to the outlet. This zone can be seen in Figure 4.12. For this case the vapour fraction measurements are also averaged over all time-steps after initialization, in the same way



Figure 4.11: *The 2D model with the mid-stream zone over which the vapour fraction was measured marked. It is placed somewhat downstream from the venturi throat as the obstruction object will be considerably elongated as part of the first parameter study.*

as described above, to avoid large oscillations due to the fluctuations in the flow.



Figure 4.12: *The 2D model with near-wall zone where the vapour fraction is to be minimized marked in red.*

4.3.5 Database generation

When using second level optimization you need to create a solver approximation on the basis of the experiments conducted. This solver approximation, in this case the neural network, is then in turn utilized for the actual optimization. To train the neural network a database is created on the basis of the simulations performed.

The database consists of information relevant for the optimization, i.e. parameter configuration and output data from the simulation. So for each case the configuration sampled was paired with the calculated output values, see Section 4.3.4, to make it possible to analyze the influence of the individual parameters on the results.

4.4 Optimization

The optimization was conducted using neural network methods presented in Section 3.4.4 and a Particle Swarm Optimization method adapted for multiobjective optimization.

4.4.1 Neural network

The neural network is trained with a Levenberg-Marquardt back-propagation method and the training error is measured by the mean square of output errors. To avoid overtraining the network, regularization was used for all available samples. This is done to get more accurate results with a smaller database, compared to using early stopping.

4.4.2 Optimization algorithm

The optimization is based on a multiobjective extension to the PSO algorithm, see Section 3.4.5, proposed by Coello et al. (2004). It is named *MultiObjective Particle Swarm Optimization (MOPSO)* and was found to compare favourably to several other multi-objective optimization methods in that it performed well at reasonably low computational costs.

It implements the same basic idea as the PSO method, but it considers that a global optimum cannot be achieved, rather each particle should be moved in the direction of the Pareto front. The method is summarized in Lundberg (2014, Chap 4) as

1. Create particles with random position on search domain.
2. For every generation:
 - (a) Use solver approximation, i.e. Neural Network, to compute average vapour fraction on both zones.
 - (b) Find Pareto front.
 - (c) Choose particle leaders from Pareto front. Leaders differ between particles depending on place in domain.
 - (d) Move the particles in the direction of the leader that was assigned.
 - (e) Randomly mutate position of some particles as local search.
3. Return Pareto front from the last generation as solution.

5

Results

IN THE FOLLOWING chapter the results obtained in the two parameter studies are shown.

5.1 Investigation 1: Six parameters

The largest study that was carried out within this project was a six parameter investigation testing several geometrical parameters as explained in Section 4.3. In the following section results and considerations from this investigation are listed.

5.1.1 Parameter influence

The most important result to take from the investigation was the type of influence the parameters had on the results. It means analyzing whether a change in a certain direction of a parameter has a positive or negative impact on the objective function. For multiple objectives this means that the same parameter can have a positive and a negative influence at the same time, and therefore the results for each objective are shown in figures 5.1 and 5.2 for mid-stream zone and near-wall respectively.

Pressures

The large influence of the outlet pressure is ostentatious. It has a large negative influence on the vapour fraction both near the wall and in the mid-stream zone. This is reasonable considering that the cavitation collapse will increase when the surrounding pressure

Table 5.1: The number assigned to each parameter in the plots showing parameter correlation. For details on the parameters see Section 4.3.

ID	Parameter
1	Curvature length
2	Obstruction length
3	Obstruction ratio
4	Throat radius
5	Inlet pressure
6	Outlet pressure

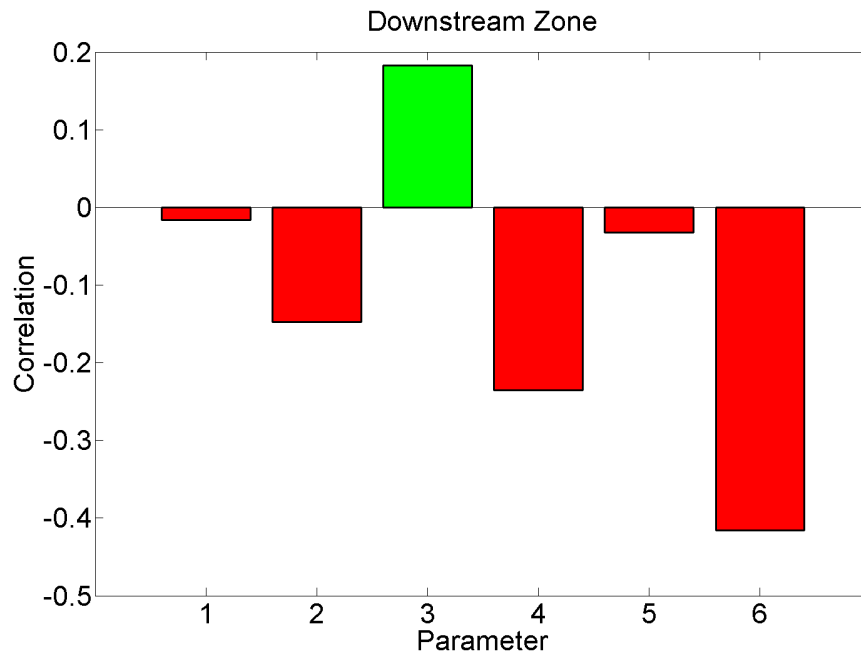


Figure 5.1: Correlation between the parameters and the vapour fraction for zone in the centre of flow. As this objective should be maximized a positive correlation is coloured green and a negative correlation is coloured red. For information on which parameter corresponds to which number see Table 5.1.

increases. Furthermore an increase in outlet pressure also leads to an overall decrease in driving pressure over the pipe and lower velocities in the venturi throat which in turn lowers the pressure drop in the venturi. This means that the total amount of cavitation in the system will decrease when the outlet pressure is increased. To further analyze this parameter a large number of sample points from the solver approximation are plotted in Figure 5.3. The downward trend becomes more clearly visible, and this is a key parameter

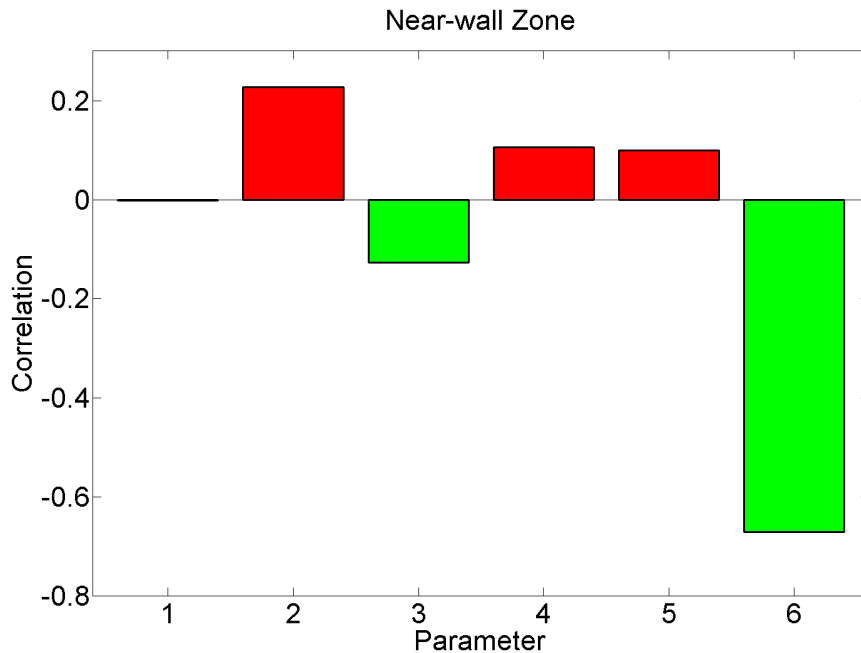


Figure 5.2: The correlation between each parameter and the vapour fraction in the zone near the wall. A positive correlation indicates an increased value of the parameter yields a higher value for the objective function and vice versa. As the target is to minimize vapour fraction near wall a negative correlation is considered more optimal, hence red colour for positive correlation and green for negative correlation. The parameter corresponding to a certain number can be seen in Table 5.1.

for controlling the cavitation. It is also key for controlling the intensity of the cavitation collapse, as the intensity will increase with increasing surrounding pressure. As intensive bubble collapses are important for fibre treatment the pressure in the downstream zone must not be too low.

This view is confirmed by the fact that outlet pressure also plays a very important role in limiting near-wall cavitation, which can be clearly seen in Figure 5.2. The same physical mechanisms are at play here, but for this parameter the decrease in vapour fraction is seen as a positive thing. This, together with increasing intensity of bubble collapse, is the main rationale behind actually increasing the outlet pressure for the second part of the study, despite the positive effect on mid-stream cavitation.

The inlet pressure however seems to have very little influence on the amount of cavitation downstream the venturi, indicating that it is not the limiting parameter and that the venturi effectively shields the downstream volume from influence of the inlet pressure.

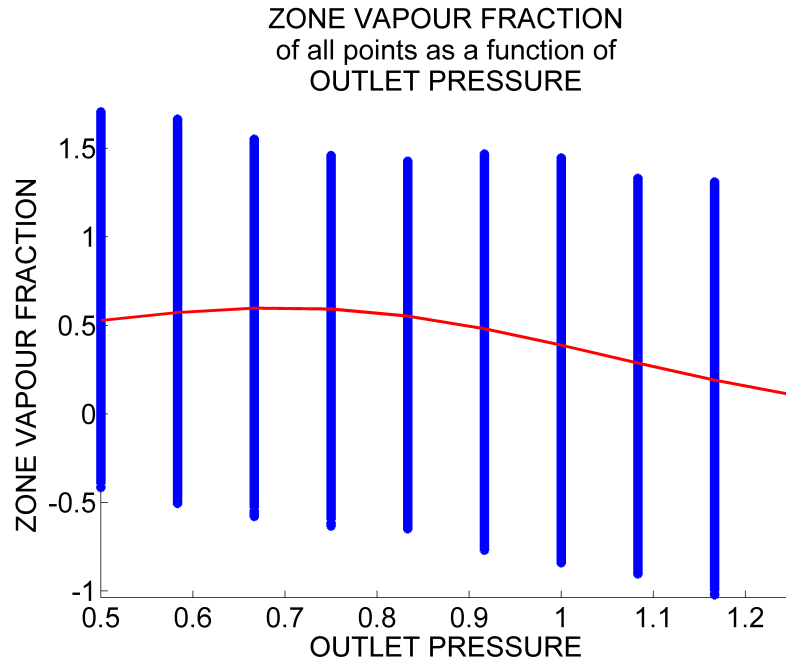


Figure 5.3: The vapour fraction in the mid-stream zone plotted against the outlet pressure for a large number of solver approximation samples. The blue bars correspond to values for each sample point of outlet pressure and the red line shows the mean value. The decreasing trend can be seen.

Curvature length

As the pressure may be regulated independently of the venturi shape, further attention should be directed to geometrical parameters of the investigation. As can be seen in Figure 5.1 curvature length has very little influence on the vapour fraction in the zone, it decreases slightly with increasing curvature length.

From Figure 5.2 it can be seen that the curvature length also has a small negative influence on near-wall cavitation, i.e. increasing the curvature length slightly increases the near-wall vapour fraction.

Obstruction length

From Figure 5.1 it seems that the negative influence of increasing the length of the obstruction is significant. However looking in more detail at the impact of the length of the obstruction, see Figure 5.4, the trend is less clear cut. The trend is only clear for values near the baseline, increasing the obstruction further downstream has little effect on the amount of vapour fraction in the flow. This indicates that the critical span is near the venturi throat, if the end of the obstruction is in this region the effects are clearly

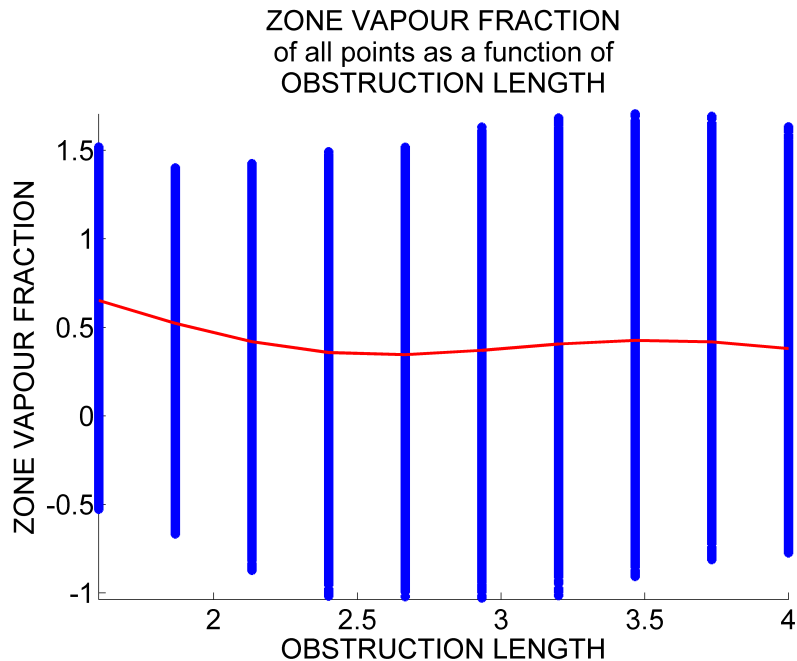


Figure 5.4: Vapour fraction in the zone behind the obstruction object plotted against the length of the same object for a large number of points from the solver approximation.

postive.

This argument is further strengthened by the results from the near-wall region, in Figure 5.2 it is noted that the obstruction length is the geometric parameter with the largest influence on near-wall vapour fraction. If the length of the obstruction is increased the amount of near wall vapour increases significantly, which further reinforces the argument that the obstruction should be kept within the venturi throat.

Obstruction ratio

Analyzing the influence of the obstruction ratio it can be seen quite clearly that increasing the ratio of the throat that is blocked by the obstruction also increases the vapour fraction in the mid-stream zone. This is reasonable as increasing the ratio of the throat that is blocked decreases the free flow passage and increases velocity of the liquid when passing through the venturi. This causes larger pressure drop and increases the amount of cavitation.

Interestingly the obstruction ratio has a positive influence on the near-wall vapour fraction as well, i.e. the vapour fraction decreases with increasing obstruction ratio. This is probably because the flow is pushed towards the wall and tends to attach, which creates what can be likened to a protective film on the wall, shielding it somewhat from

cavitation.

Throat radius

For the throat radius the effect is the opposite of the effect of obstruction ratio. This is to be expected as the two parameters are effectively cancelling each other out. Thus increasing the throat radius decreases the amount of mid-stream cavitation.

However the effect on the near-wall cavitation is next to negligible, indicating that this parameter could be fixed, and the flow controlled by varying only the obstruction ratio.

5.1.2 Pareto front

The multiobjective optimization yields a Pareto front of non-dominated configurations, see Section 3.4.2. For the first investigation the Pareto front can be seen in Figure 5.5. Here one can note that values are unrealistic due to the high standard deviations in the results creating an extremely volatile response surface which needs higher database resolution to be able to make accurate predictions from a solver approximation.

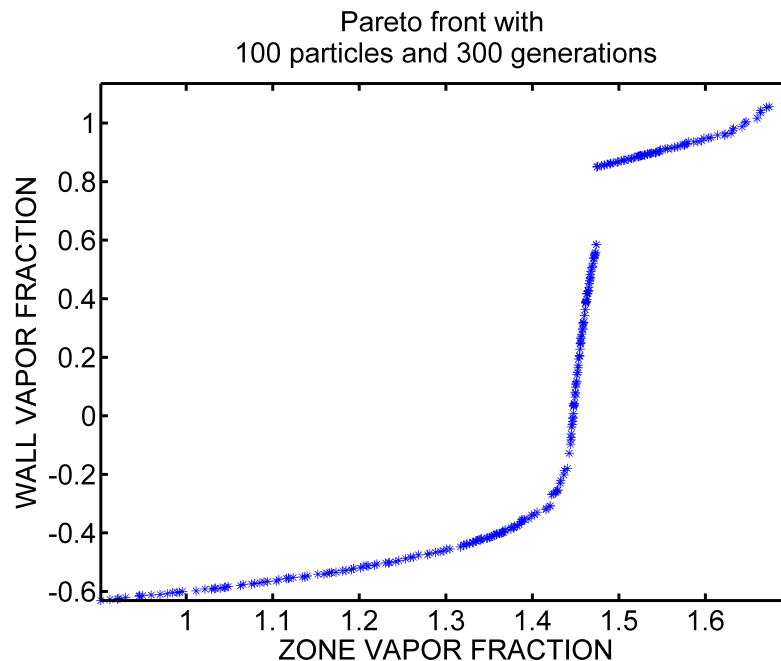


Figure 5.5: *The Pareto front yielded from the optimization of the first investigation. The jump in the front indicates that for some critical points the mid-stream vapour fraction cannot be enhanced without significantly increasing the near-wall vapour fraction.*

5.1.3 Geometry enhancement

The optimization tool returns an optimal design based on the solver approximation. In practice this means choosing a certain non-dominated point on the Pareto front according to the priorities of the design. In this case the choice was made where the gradient of the Pareto front is small to avoid large oscillations of results around the chosen point. It must however also consider desired results, and in this case it was decided that minimizing the cavitation along the wall was especially important. So the optimal value was chosen where the approximated wall vapour fraction was 0 or below, which yielded the configuration seen in Table 5.2.

The trends of parameter influence are reflected in this result and many of the values are near the maximum allowed values for that parameter. An extreme value is reached for *outlet curvature*, *obstruction length*, *obstruction ratio* and *inlet pressure* and very nearly for *throat radius*. For all these parameters the maximum value of mid-stream cavitation was reached near an extreme value for the parameter.

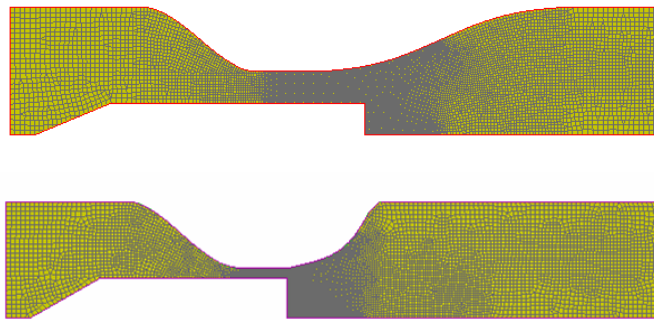


Figure 5.6: Comparison of the baseline geometry and the optimal geometry obtained from optimization of investigation 1. The baseline on top and the optimized case below. The pipe section downstream has been removed to more clearly illustrate the changes in the throat region.

The near maximal parameter change also suggests that further improvement of the model could be possible if it allows for larger variations in parameter values, or that the parameter has so small influence on the objective function that it can vary almost without consequence. This is reflected in the second investigation where certain parameters are varied within a different range while others are locked entirely.

An illustration of the baseline case and the optimal configuration obtained in this investigation can be seen in Figure 5.6. It can be noted that the cross-section of the venturi throat is significantly smaller than for the baseline, and that the expansion of the throat a lot more rapid than for the baseline case.

Table 5.2: The normalized changes to values of the investigated parameters, as suggested by optimization during investigation 1. Values are normalised, see Section 4.3.

Parameter	Change
Outlet curvature length	-1.2
Obstruction length	-0.4
Obstruction height	+30 %
Throat radius	-0.072
Inlet pressure	-0.5 bar
Outlet pressure	-0.19 bar

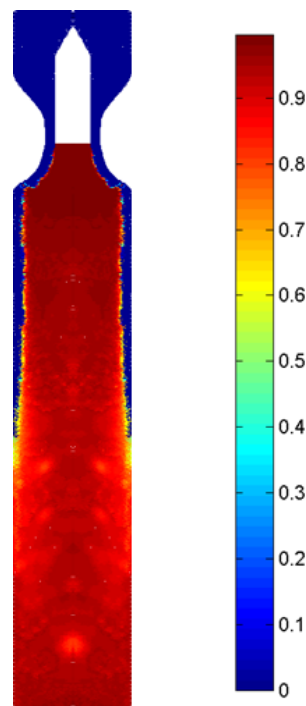


Figure 5.7: The Amount of vapour fraction plotted for the optimal configuration in substudy 1. To visualize axisymmetry the plot has been mirrored. It is also rotated to correctly describe the flow direction. The colour bar indicates amount of vapour fraction.

Verifying optimal case

The optimal case was tested by simulating the case with the same settings that had been utilized for the larger investigation. This was particularly important considering that the predictions for vapour fraction from the optimization were non-physical with values not lying between 0 and 1, see Table 5.3. This meant that optimization predictions did

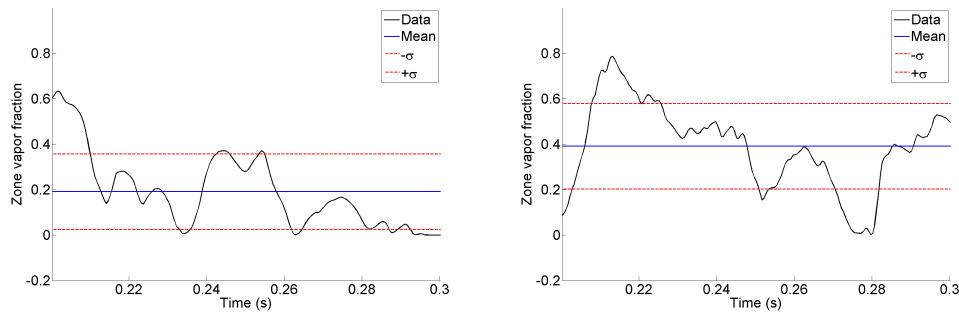


Figure 5.8: The vapour fraction in the mid-stream zone for two random parameter sample configuration plotted against time.

Table 5.3: The values for the two objective functions calculated for the baseline case and the optimal case in investigation 1. The mid-stream objective is significantly improved, but at the expense of significant increase in near-wall cavitation.

Case	Mid-stream vf [%]	Near-wall vf [%]
Baseline	0	1.8
Prediction	90	-63
Optimum	94	59

contain some errors, and by simulating the case the error margin could be determined. Comparing the simulation with the prediction it can be seen that the prediction for the mid-stream vapour fraction is within reasonable error margin, but the near-wall vapor fraction is not well predicted. The reasons for this deviance are discussed in Chapter 6.

With the mid-stream vapour fraction considerably increased the optimization tool has achieved an improvement in parameter one, but at the cost of a decline in parameter two, where a significant increase is noted.

This is largely due to the increased overall vapour fraction for the entire pipe-section and the lowered outlet pressure certainly contributes to bringing a larger volume below critical pressure. With the outlet pressure under 1 bar the pressure recovery is much slower and almost the entire zone downstream the venturi is gas phase, see Figure 5.7. This is a reason for raising the maximum outlet pressure for substudy 2, to guarantee that the entire flow does not cavitate.

5.1.4 Convergence study

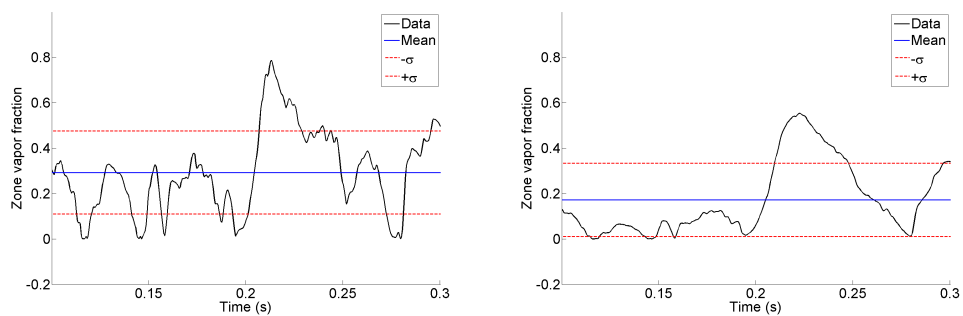
As all simulations are transient and the system is noted to be highly unstable the residuals and convergence of the study must be scrutinized in order to determine the reliability of

the results.

The first consideration for the larger investigation was to assess the fluctuation of the vapour fraction over the time of the simulation. The process fluctuates with time, so this becomes a key factor for reliability. In Figure 5.8 two instances of this can be seen for the mid-stream zone. It is noticeable that the fluctuations cannot be said to be cyclic for this sample size, i.e. the mid-stream zone, rather they seem stochastic. The limitation in time-steps means that a longer cycle cannot be entirely ruled out, but the fluctuating behaviour of the flow seems partly offset by the amount of time-steps over which the mean is calculated, making the output representative of the measurement series.

The irregular nature of the vapour fraction means that the standard deviation from the mean for the measurement series is rather large, and this can be seen clearly from the two samples shown in Figure 5.8. The high fluctuations of the cavitation activity could lead to uneven fibre treatment, so the residence time of the fibres within the reactor cavitation zone must be large enough to compensate for this. This could pose an important question for future simulations and experiments in establishing timescales for both cavity fluctuation and residence time of fibres with greater certainty.

For comparison the same case as in Figure 5.8 was tested for a somewhat longer time-span, and measurements were also taken on a larger mid-stream zone. The near-wall zone was not enlarged, but was also tested for a longer time-span. These measurements however provide little to no extra information about any longer cycles in flow, see Figure 5.9. It can be noted that measuring over a larger zone evens out the spikes and lowers the peaks, suggesting that the cavitation activity is focused in the zone defined for the objective function. This is further emphasized by the considerably higher average in the smaller zone than in the larger zone.



(a) Vapour fraction in the standard mid-stream zone during a longer time. (b) Vapour fraction in the mid-stream zone plotted for both longer time and larger zone.

Figure 5.9: The vapour fraction plots from reference run, with added time-steps compared to Figure 5.8.

Table 5.4: The number assigned to the parameters in the parameter correlation plots for the four parameter study. For details on the parameters see Section 4.3.

ID	Parameter
1	Obstruction position
2	Obstruction radius
3	Inlet pressure
4	Outlet pressure

5.2 Investigation 2: Four parameters

The second investigation utilizes input from the first investigation to lock two parameters and study only four parameters deemed to be the most important for the objective function. The analysis of the first investigation also yielded a slight alteration on how the parameters were defined. The length of the obstruction seemed to be less important for the objective than the position of the obstruction. This is also interesting as it could become a control parameter where a mechanism could be installed to make the obstruction mobile.

Both the curvature length and the throat radius were locked as their influence was not substantial. Furthermore the more important part of the influence of the throat radius, i.e. the cross-section of free flow through the throat, is still investigated when varying the radius of the obstruction object.

Furthermore input from project management had requested the pressure be kept at or above atmospheric level to increase the intensity of the cavitation collapse, so the sample span for the pressures were adjusted upwards for both inlet and outlet pressure.

5.2.1 Parameter influence

The impact of the parameters on the two targets can be seen in Figure 5.10 where the correlation between parameters and vapour fraction in the mid-stream zone and Figure 5.11 for the correlation between parameters and vapour fraction along the wall of channel.

Obstruction position

It is noted that the mid-stream zone vapour fraction is negatively impacted by moving the obstruction in the positive x-direction, i.e. downstream. At the same time the near-wall vapour fraction is also increased by the same change. This suggests that the cavitat-

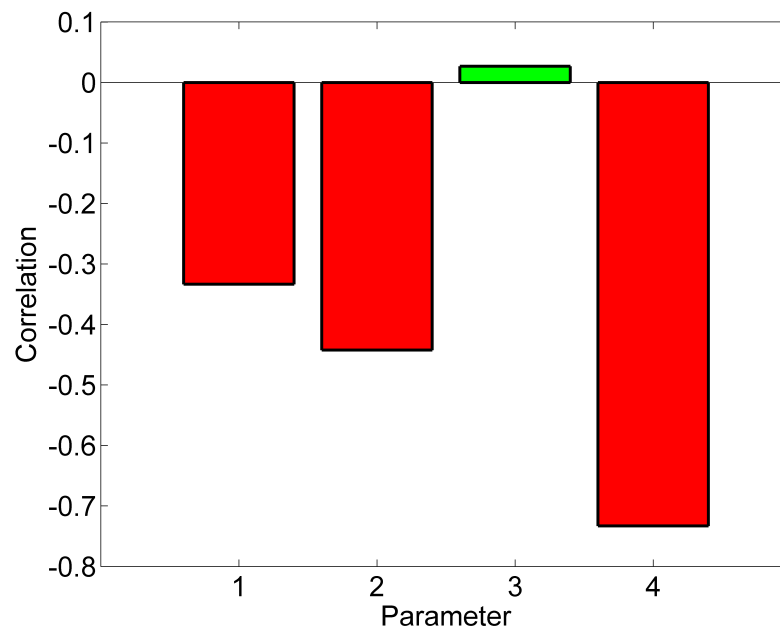


Figure 5.10: Influence of the four parameters in the second parameter study on the vapour fraction in the mid-stream zone. As the target is maximizing this value, a positive influence, i.e. increase of parameter leads to higher vapour fraction, is coloured green. Conversely a decrease is coloured red.

ing flow is pushed towards the wall of the pipe when the obstruction is moved downstream.

Obstruction radius

The vapour fraction is increased overall, both for the mid-stream zone as well as the near wall zone with decreasing radius. However it can be observed in Figure 5.13 the relation is nonlinear for the vapour fraction near the wall. It can also be noted that for increasing radius of the obstruction object, values are rather constant.

Pressure

Inlet pressure again has a very limited effect on both mid-stream and near wall cavitation, presumably because the obstruction and venturi shields the pressure field downstream from influence of the inlet pressure. The outlet pressure however retains a negative effect on the amount of cavitation both near the wall and mid-stream. This result is to be expected, but to make the cavitation collapse more intense it should still be kept fairly high.

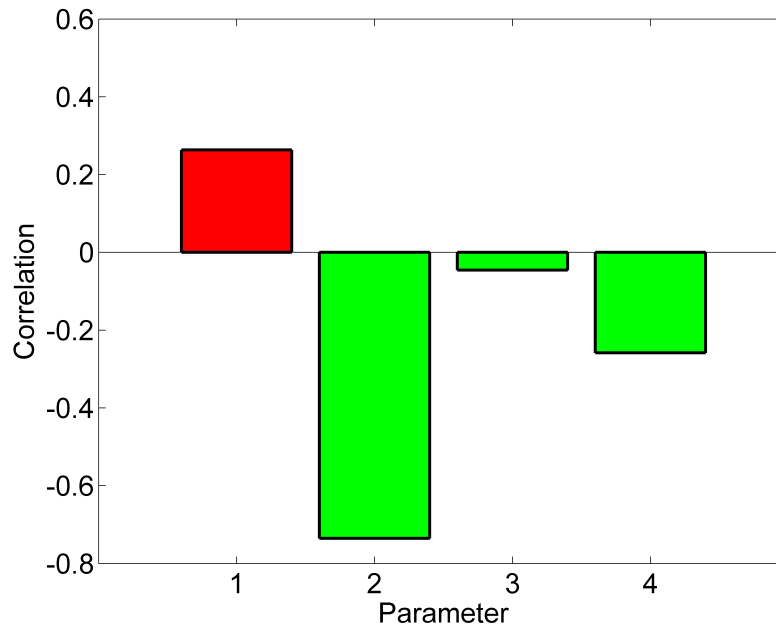


Figure 5.11: *The influence of the parameters in the second parameter study on the vapour fraction near the wall. colouring reflects the goal of optimization, i.e. reduction is considered good and is coloured green. Correspondingly an increase is coloured red.*

Table 5.5: *The optimal values for the investigated parameters as suggested by optimization on investigation number 2. All values normalised, see Section 4.3.*

Parameter	Change
Obstruction position	-0.1
Obstruction radius	-0.031
Inlet pressure	+1.25 bar
Outlet pressure	0 bar

5.2.2 Geometry enhancement

The optimization based on the second investigation yields a near maximum negative displacement of the obstruction object, with the radius kept at nearly baseline level. The baseline and optimal configurations can be seen in Figure 5.14. The changes in the parameters are also listed in Table 5.5 together with the predicted values for the two objective functions. Here a weakness in the optimization can be observed as it predicts a negative value for the near wall vapour fraction. This is because the optimization is unbounded and can assume any value on the solver approximation. Therefore the optimal case is run and tested, see below.

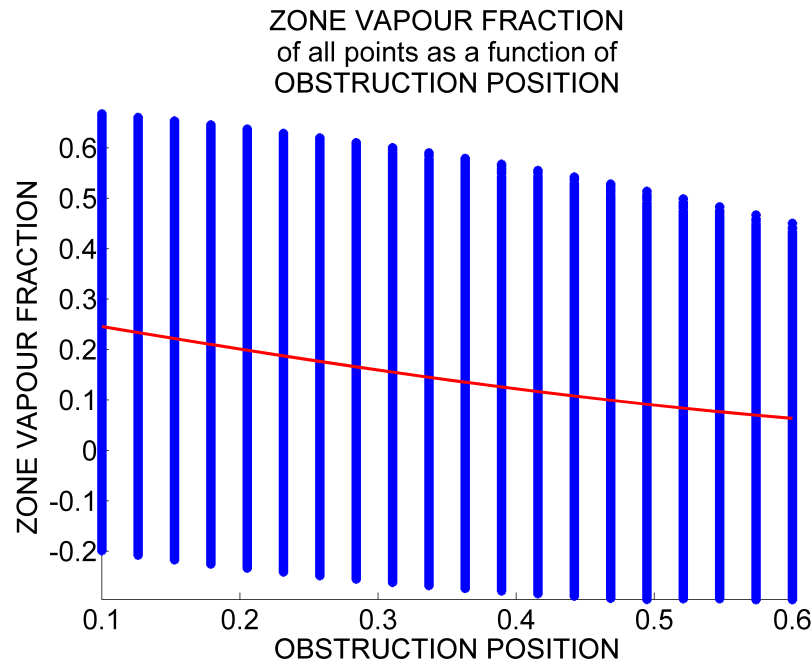


Figure 5.12: *The vapour fraction in the mid-stream zone plotted against the position of the obstruction object. The declining trend in vapour fraction is clear, indicating the obstruction object should be placed upstream of the venturi throat exit.*

The small alterations made indicate that the new baseline design set for the second investigation is an improvement on the previous designs, and that the parameters need not be severely altered.

Verifying optimal case

The suggested optimum was generated and tested using the same algorithm as for the parameter study. It was especially interesting given the unphysical predictions given by the optimization study. The output was a clear improvement on the baseline case with the vapour fraction in the mid-stream zone more than doubling from 42% to 94%, while the near-wall vapour fraction decreased slightly from 5.3% to 3.4%. Results can be seen in Table 5.6.

In summary this can be said to indicate that the optimization tool works in so far as improving the configuration, but its predictions on untested configuration seems rather unreliable. The prediction should therefore be interpreted on a qualitative rather than a quantitative level.

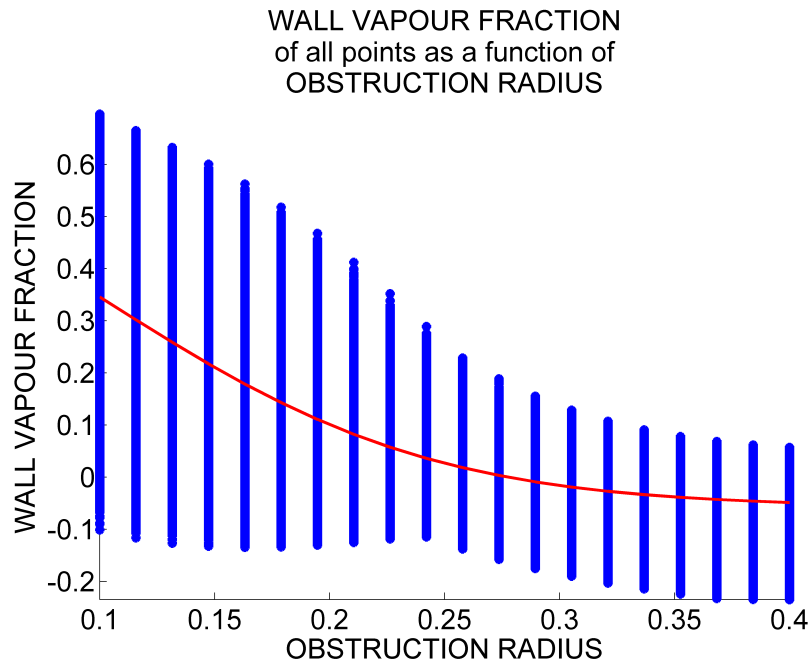


Figure 5.13: *The vapour fraction near the wall plotted as a function of the radius of the obstruction. This indicates that the obstruction radius should be increased to avoid near-wall cavitation.*

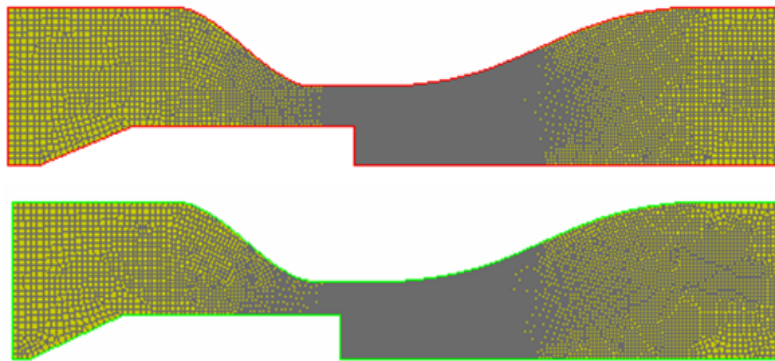


Figure 5.14: *Comparison of the baseline geometry and the optimal geometry obtained from optimization of investigation 2. The baseline on top and the optimized case below. Only small alterations produced in optimization, but not that the obstruction is moved slightly upwards and upstream.*

5.2.3 Convergence study

Just as for the first investigation the results tend to oscillate quite heavily, and the convergence and stability must be examined. In Figure 5.16 it can be noted that the

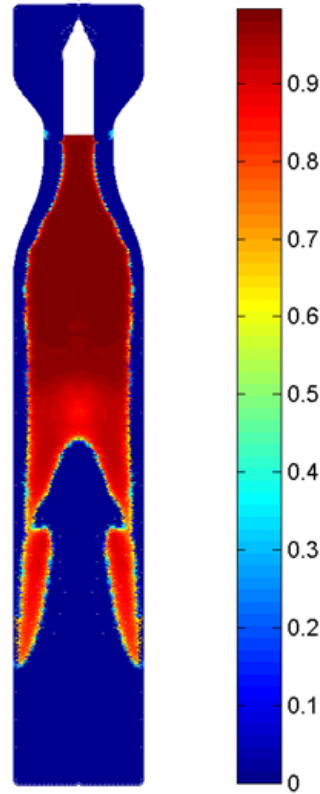


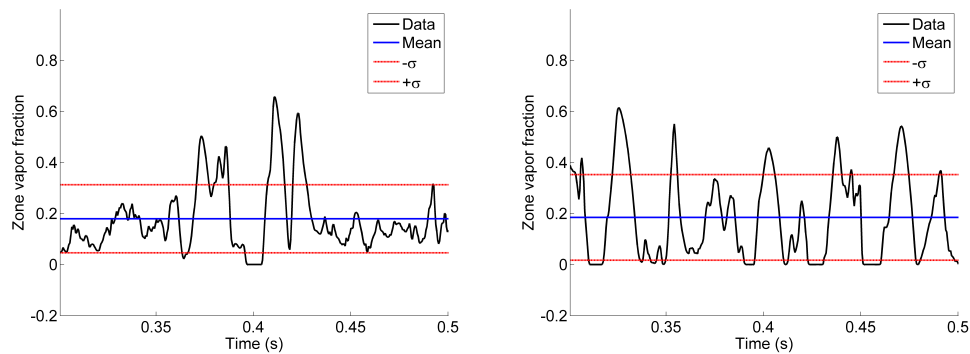
Figure 5.15: The vapour fraction for the optimal configuration yielded from substudy 2. Mirrored to reflect axisymmetry. The attached flow of water along the wall prevents the cavitating flow from reaching the wall which well reflects the targets of optimization. It can also be noted that for this time-step a vapour bubble is released from the rest of the cavitating zone.

Table 5.6: The values for the two objective functions calculated for the baseline case and the optimal case in investigation 2. As seen both objectives are enhanced in the optimal case compared with baseline.

Case	Mid-stream vf [%]	Near-wall vf [%]
Baseline	42	5.3
Prediction	54	-16
Optimum	94	3.4

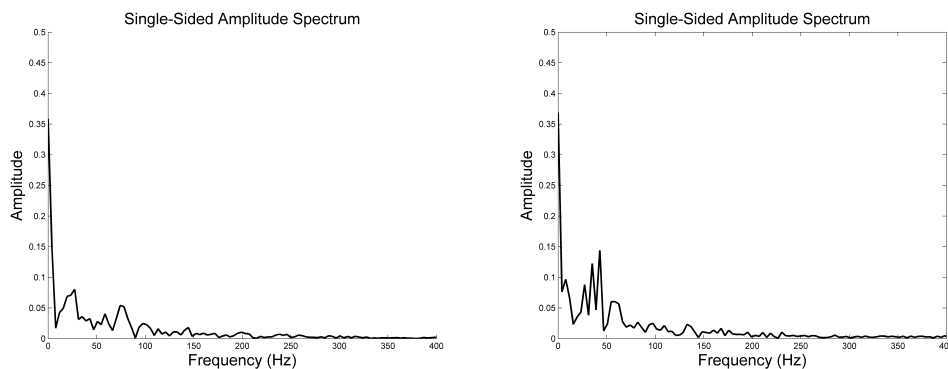
random oscillations still occur in the simulations. The oscillations are quite large and seem to occur randomly or quasi-randomly.

Analyzing the cases with Fast Fourier Transform of the data to retrieve any dominant frequency in the fluctuation yields some peaks at frequencies around 35 Hz and 45 Hz for the second case, see Figure 5.16. This corresponds to period of roughly 0.03 s and



(a) Sample case 1. Vapour fraction in mid-stream zone.

(b) Sample case 2. Vapour fraction in mid-stream zone.



(c) Sample case 1. Fast Fourier Transform of vapour fraction data.

(d) Sample case 2. Fast Fourier Transform of vapour fraction data.

Figure 5.16: Average vapour fraction plotted against time for two random samples in the four parameter study. Directly underneath is the Fourier transform of the data plotted against frequency. Fluctuations are quite quick and standard deviations are fairly large. No clear results can be deduced from the Fourier transformation implying a random nature of the fluctuations.

0.02s respectively, which is well within the sample time of 0.2s. For the first case almost no clear frequencies can be noted except for 0 Hz which has no physical meaning. The fact that it varies between different simulation also indicates random rather than deterministic frequencies of vapour fraction variation.

The residuals of the calculations are notoriously high for cavitation calculation, especially continuity becomes sensitive given the mass transfer between the phases. For the most cases the continuity residual hovers around the 10^{-2} mark, which must be considered higher than desired. However the limitations in computer resources meant that somewhat higher but stable residuals are acceptable to be able to run more time-steps and thus minimize the influence of random events on the results.

5.3 Summary

To summarize, the two studies show that outlet pressure and obstruction configuration are the most critical parameters to control the amount and position of cavitation bubbles downstream the venturi. The inlet pressure is shielded and has little influence on the cavitation. This is as long as the pressure is high enough to accelerate the flow to the point where cavitation is induced. The outlet pressure however is important for the amount of cavitation, and need to be kept fairly high to limit near-wall cavitation and to ensure the intensity of bubble collapse.

In general one can conclude that the radius of the obstruction object should be increased to reduce the amount of near-wall cavitation, but this also reduces the mid-stream cavitation, so a working compromise needs to be found. The position should be moved towards the inlet both to increase mid-stream cavitation and reduce near-wall cavitation.

6

Discussion

IN THIS chapter the results obtained are analysed and discussed.

6.1 Error margin

The error margin of all the performed studies in this thesis is quite high, a problem that is very hard to resolve given the unstable physics of the problem and the scope of the study. To be able to conduct a detailed parameter study it is important that a considerable number of simulations can be performed. This means that in this work due to the limitations with respect to time and computational resources the simulations were executed for a shorter time period and for fewer sample configurations.

The trade-off between accuracy and speed is fundamental in all computational modelling, and it is important that one pays significant attention to finding a good balance between the two. When doing so one must also consider the needs for the specific study. For this particular case the complexity of the researched problem and difficulty to predict the behaviour of the system without running full scale simulations meant that this became especially important. On the one hand it is important that the results are accurate and reliable, while on the other hand it is important to test as broad a spectrum of parameter settings as possible. Otherwise an important parameter might be overlooked and locked at a sub-optimal value without sufficient investigation. It is also important to know that this study is at an early stage in a larger project, and the results from this study are not intended to form the basis of a prototype. Instead they should be used as an indicator of which direction to go with the future development of the project and give a better understanding and feeling for the system. This is important when the behaviour of the system is non-linear and non-intuitive.

6.2 Source of errors

In a study that consists of several layers of models it is important to note that each of these models are approximative and have their own error sources. This means in principal that any errors in output results from optimization could be induced from either one of CFD simulations, neural network solver approximations or optimization.

6.2.1 CFD simulations

To find a working compromise between the need for accuracy and the need for speed in the simulation was one of the major time consuming tasks. As stated above, a fairly large error has been tolerated in these calculations. This was done partly because theory and literature (Lundberg, 2014) suggested quite high precision and robustness for the solver approximation and optimization methods that have been implemented in this thesis.

The biggest problem for these simulations was minimizing the residuals of continuity and vapour fraction, which are also coupled to each other. The complex case of mass transfer between two phases where density varies by about three orders of magnitude requires a very fine resolution in both space and time to be accurate when performing transient simulations. So for the mesh and timestep decided on, see Section 4.2, the residuals were typically on the scale of 10^{-2} for continuity and 10^{-3} for vapour fraction with all other residuals on the range from 10^{-6} to 10^{-8} for a typical run. The notion that these high residuals were coming from the multiphase modelling and phase transition was confirmed by analyzing the residuals for non-cavitating cases, ie where critical conditions for cavitation were not achieved. For these cases continuity residuals could go down to about 10^{-12} and vapour fraction residuals were non-applicable as the flow was single-phase.

Is it advisable to resolve the case finer both in space and time to further reduce these residuals and obtain better results? Firstly this would mean much more time-consuming simulations for a case that can be considered feasible, see Section 6.4. Secondly, when further analysis were conducted, it was found, the same did not have a significant impact on the end results. For instance, despite the high residuals for continuity, the mass imbalance between inlet and outlet were below 0.1% for all analyzed cavitating cases. Furthermore the grid independence study suggested that the essential behaviour of the objective function, i.e. the distribution of cavitation, was sufficiently resolved in the 13k-cell mesh studied. The cell measurements used for this cell then formed the basis for all simulations. In the grid independence study the general shape of the flow and cavitating parts of the flow were also visually analyzed, and although a finer mesh naturally produced more accurate results when it comes to describing turbulence and location of cavitation zones the general shape and distribution in the flow were satisfyingly captured by the coarser mesh as well.

So despite causing higher than desired residuals, indications are that the objective functions were not significantly altered by the residuals. Unfortunately more exact testing of this was impossible to conduct because of the limitations in computational resources, so an exact value of the error could not be obtained. But based on the results of grid independence study, the errors are within acceptable margins for a pilot study designed to find only general behaviour of the system, rather than exact solutions.

6.2.2 Neural network solver approximation

The error generated in the neural network solver approximation can be characterized mainly as the error in predicted results from a configuration, and the actual result when the configuration is simulated. As seen in the previous chapter this error can be quite large.

These errors can be tracked back to the training of the network, which in turn is dependent on database size, training method and non-linearities in response surface. Given the rather small database of 65 cases for 6 parameters a review of literature suggested the training method to be Bayesian Regularization, see Chapter 3. However it is also important to note that there is a degree case specificity to the number of sample points needed to construct an adequate database. For the studied case where solutions are highly non-linear and measurements vary over time the response surface will be quite complex and might need a higher resolution for the neural network to be able to yield accurate predictions. This would require more simulations and therefore it was decided to accept some prediction error as long as the underlying trends could be accurately described.

To test whether this level of reliability had been achieved the same database was approximated using different neural networks. This was done using the same method and size of database multiple times, to test if the neural network converged to similar solutions for every initialization, i.e. multiple tries with the same settings in MATLAB. The result can be seen in Figure 6.1 where it is noted that the differences are not insignificant between the different cases, but they all capture the same type of trend and are not randomly distributed.

To gain further insight into the influence of the neural network the parameter correlations were tested for two different neural networks, the comparison can be seen in Figure 6.2. From this comparison one can note that the different networks yield somewhat different results, most ostentatious is the change in sign for parameter 1. The other parameters vary somewhat in the correlation, but the principal effect on the system remains the same. The reason for this change is unclear, but could be due to the relatively small influence of this parameter and the pretty small database size, which makes the neural network more prone to converging to different solutions for a complex surface. It must therefore be noted that the solutions are not independent of the neural network, but differences are within acceptable error margin. Specifically for parameter 1, curvature

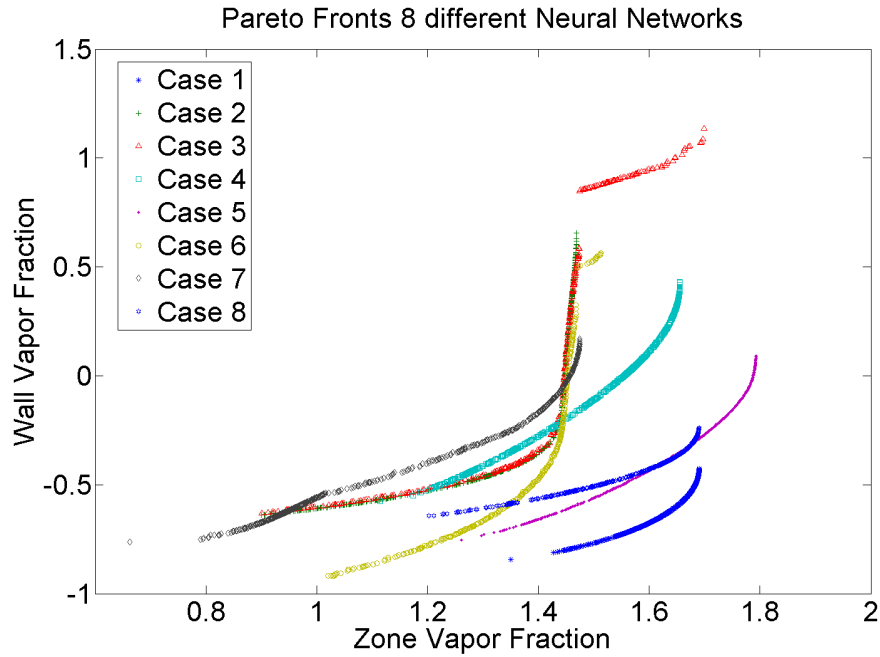


Figure 6.1: Eight different Pareto fronts created using 100 particles and 300 generations optimization, but with the neural network reinitialised for each case.

length, the uncertainty of the results and relatively small influence meant it was locked at the baseline value for later investigations.

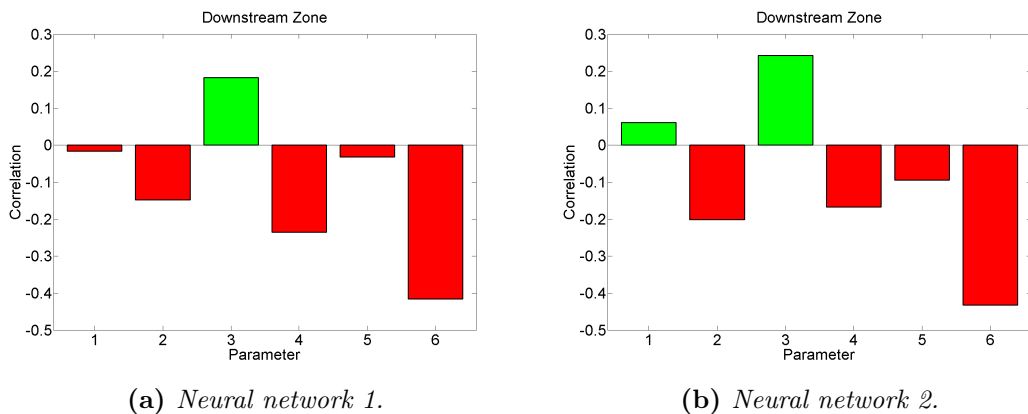


Figure 6.2: The parameter correlation for two different neural networks. Some differences occur, most notably in the first parameter, the curvature length, which changes sign. But absolute value is small for this parameter in both cases.

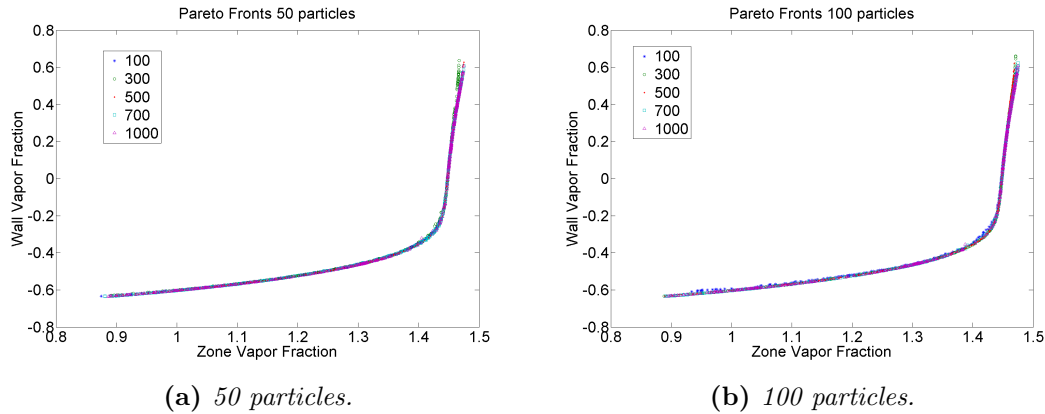


Figure 6.3: Test of different number of generations for optimization. On the left with 50 initial particles, and 100 initial particles on the right. All tests are done with the same neural network. It can be seen that they have converged to the same Pareto front with very small deviations.

6.2.3 Optimization

The optimization can give rise to an error by finding different solutions for the same solver approximation. This can be described by the same neural network and optimization setting yielding different Pareto fronts. However, when accuracy of prediction is not needed, the most important measurement is the relative impact of the different parameters. That means that it is sufficient that the general shape of the Pareto front is constant, and that the parameter influence on the objective functions is independent of the optimization.

This was tested by running the optimization for different settings regarding number of initial particles and number of generations, seen in Figure 6.3. This study shows that the optimization is stable as long as the neural network is kept constant, and seemingly regardless of both amount of particles and generations it converges to a similar Pareto front. From this the conclusion can be drawn that the results are next to independent of the optimization parameters, at least for the tested range.

Judging from this, the results yielded from optimization using 100 particles and 300 generations are reliable enough to draw conclusions about the system behaviour and influence of the parameters on objectives. However, what cannot be done, is drawing specific quantitative conclusions based on the optimization as the predictions obtained are often non-realistic, therefore every configuration suggested from the optimization tool should be verified by simulations before any further conclusions are drawn.

6.3 Accuracy of results

Acknowledging the error sources in the study, the large residuals of the simulation runs and the difficulties of the solver approximation to respect the physical boundaries of the result space, one should be careful in drawing conclusions from the results obtained. But this does not mean that the results cannot be used and analyzed.

The test runs with the optimal configurations suggested by the two investigations have yielded interesting results and vastly improved results in comparison with the baseline cases that formed the basis of each investigation. This is an indication that the method works to the degree that it improves the system and the design, but not to the degree where accurate predictions can be made using the optimization tool and solver approximation. In short one can say that predictions can be made on a qualitative but not on a quantitative level.

This is also within the aim and scope of the study, i.e. to find a better baseline for the continued research and providing information on the behaviour of the system and influence level of different parameters.

6.4 Simulation time consumption

Computational resources were limited to a four-core desktop computer with effectively unlimited availability and a multiple CPU (16, 32 or 48) cluster with limited availability. This meant that simulation duration could vary quite heavily depending on availability of CPU cluster, an analysis run according to the flowchart seen in Figure 4.5 on the desktop computer took roughly 4 hours to perform. This meant that performing 65 such simulations would take $\frac{65 \cdot 4}{24} \approx 11$ days. This is an important reason why the database could not be larger and the amount of timesteps simulated could not be increased. Any addition to each case would magnify 65-fold and cause considerably longer overall calculation times.

The calculations for the first investigation could be split between desktop and cluster and the time it took to obtain results was thus reduced to roughly five days, which is still high, but just within acceptable time consumption.

Once the CFD simulations were finished, the post-processing and optimization packages were run in MATLAB. The major time consumption in this step was reading the output data to create the database used in the optimization. For each simulation the output data was roughly 1 GB which was stored on a network drive, with which the communication speed varied significantly meaning it was hard to make time predictions for reading data. But typically it ranged between 1 – 3 min which meant that creating the entire database for the six parameter investigation took about two hours.

The optimization package took about 2 minutes to run on a desktop computer, which

includes both training of neural network and evolutionary optimization with 300 generations.

So summarizing it is clear that the limiting factor for the investigation is the amount, and length, of CFD simulations, especially when optimizing for a large set of parameters. This also limits the scope of the investigation both when it comes to amount of timesteps possible as well as the resolution of the mesh used making this key decisions for the feasibility of the project.

6.5 Objective function

The objective function definition is important to control the optimization, as it sets the bar for what the optimization should strive to achieve. For this study it was dictated by technical demands, the combination of wanting maximum cavitation while still not ruining the walls of the device. The only real change to these parameters that can be proposed is the size and position of the zone on which cavitation seeks to be maximized. A bigger zone may be produce more reliable results by averaging over a larger number of cells, where as a smaller zone can make it possible to be more exact in optimization and obtain a safety cushion so to speak between the cavitating flow and the wall of the device.

The proposed future design that combines sonar control with the hydrodynamically induced cavitation also demands a certain distance between the expanding part of the venturi and the cavitation collapse so that the sonar control device can be applied on a non-expanding pipe. This is important to be able to achieve standing waves etcetera for the sonar reactor.

The maximization also took into consideration the need to avoid creating a zone of pure gas downstream of the venturi, and on the latter stages of the project the wish to have higher intensity in the cavitation collapse which can be ensured by having the bubbles collapse at a higher pressure. Thus limiting the pressure drop downstream the venturi whilst still aiming for high cavitation levels pretty far downstream yields the most interesting case for the continuation of the project.

6.6 Optimal cases

The two optimal configurations obtained and tested from respective investigation gives a strong indication on which physical properties that dominate the flow.

Investigation number 1

From the first case, shown in Figure 5.7, it could be deduced that the outlet pressure is very important to control the amount of cavitation downstream the venturi. It also shows that for sub-atmospheric pressures almost the entire volume may be vapour-filled despite outlet pressure being above the vapourization pressure. This is because it keeps travelling at elevated speeds when large fractions of the flow is low-density vapour.

It also shows that the flow can attach even for rather sharp expansions of the venturi, as long as the flow velocity is not increased too much, and that the curvature at the outlet was less important than expected.

Investigation number 2

Applying the lessons learned from investigation number 1 the minimum pressure was elevated to reveal the influence of the other parameters on the flow, a visualization of the vapour fraction can be seen in Figure 5.15. It could be seen that the obstruction in the throat should be placed far upstream so that the sudden expansion of flow volume occurs at high velocities in the middle of the venturi throat. This helps achieve large amounts of cavitation that is also kept in the centre of flow more effectively than when the obstruction is moved further downstream.

Another interesting observation that was made in the second investigation was that when the obstruction was made bigger and the flow was increasingly accelerated it tended to separate from the wall and thus cavitation along the wall was increased.

7

Conclusion

CONSIDERABLE PROGRESS with regards to cavitation generation, control and design outline for venturi have been achieved. The results obtained show great promise for the future design of refiners used in paper and pulp industry in order to reduce the energy consumption.

A single phase flow optimization method has been generalized and adapted for multiphase flows. Efficient and faster parameter studies of complex multiphase flow systems is now possible and the same can be applied in a wide range of applications in the future.

The data obtained from the first parameter study was used as input data to further perform several parameter studies in series. We can conclude that the accuracy of prediction can further be improved as the results obtained in this investigation serve only as a roadmap in finding better configurations for venturi based on the positive or negative influence of each analyzed parameter.

The design configuration proposed from the second investigation shows much improved performance with respect to generation and controlling of cavitation in a venturi. On an average, the mid-stream vapour fraction and near-wall vapour fraction was 94 % and 3.4 % respectively for the optimal design compared to non existent mid-stream cavitation and a vapour fraction of about 2 % near the wall for the very first simulated case.

Parameter studies also indicates that obstruction object can be used as a control parameter for generation of cavitation by adjusting the position in the streamwise direction. Also, the outlet pressure needs to be kept at a sufficiently high level for the cavitation bubbles to collapse downstream without reaching the wall.

8

Future work

BELOW ARE the outline for future work in order to innovate and design a new refiner technology based on hydrodynamic cavitation in venturi. Also, in Figure 8.1 a summary of the future work is laid out according to Shankar et al., with the most important stages of the planned development.

8.1 Computer simulations

The development process should consist of conducting more computational simulations in order to narrow the search for an optimal design. This means that for each set of simulations, representing a step forward in the series, smaller variation of dimension of parameters should be taken into consideration and the number of parameters should be decreased.

8.1.1 3D modelling

As all simulations included in this thesis have been conducted as 2D axisymmetric to reduce computational costs, an interesting development would be to test the results from the 2D investigations in a full 3D simulation not assuming axisymmetry. Simulating a cavitating flow of pure water could serve as a partial verification of the results obtained in the 2D investigation, and could give a further indication on how to construct an optimal venturi. 3D calculations will also increase the computational effort required for each simulation and require a new way of morphing the geometry, and as such represents a big step in the development of an actual prototype.

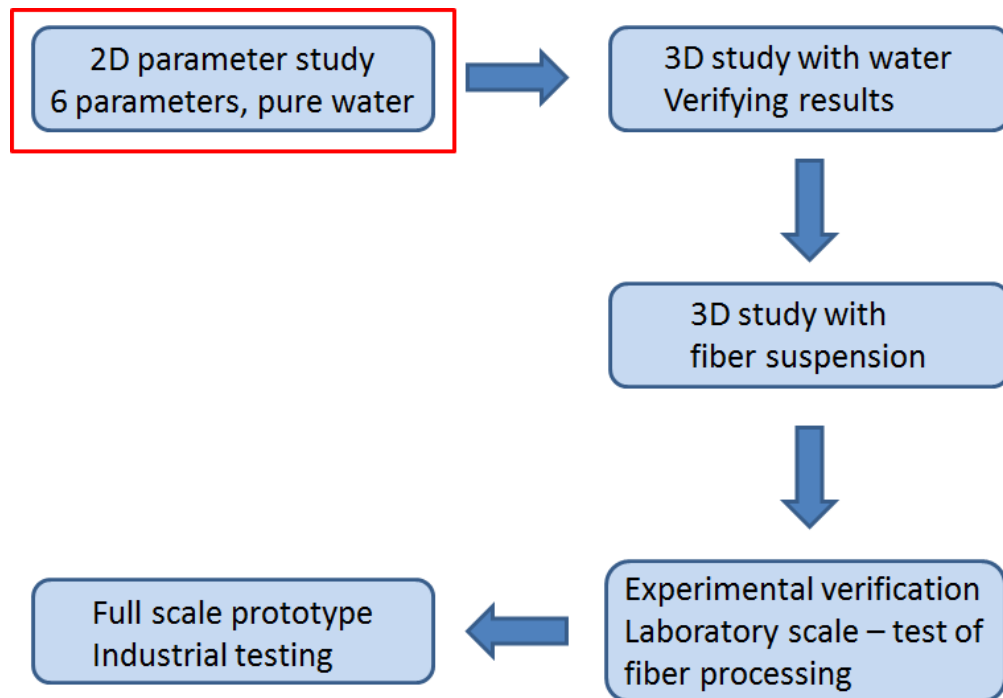


Figure 8.1: An outline of the work still to be performed within the project to develop a new type of industrial scale refiner. The current work stage, which constitutes the master's thesis is marked in red.

8.1.2 Modelling fibre flow

To investigate how cavitation bubbles will behave, the future simulations need to consider the influence of fibres within the flow. This can be done with varying levels of accuracy, from simply modifying physical properties of water to try and account for the different fluid properties of the water-fibre mixture, to actually introducing solid state fibre into the simulation.

The above mentioned points should be analyzed to be able to answer a number of important questions that cannot be addressed by simulations of just water flow in the venturi.

- How does the fibre suspension concentration affect the cavitation forming and collapse?
- How do the fibres behave when it passes through the venturi nozzle?
- How does the flow patterns change with varying concentration?
- How will the individual fibres behave in the very turbulent liquid suspension environment?

The answers to the above questions depend on the accurate modelling of fibre for a satisfactory response. The same will be one of the most important challenges for the upcoming development.

However, when fibres are modelled as solid phase particles, it means that when the flow is allowed to cavitate it will become a three-phase flow with a solid, liquid and gas phase which is a very complex system to simulate. There has been previous work conducted on fibre modelling but to the best of the author's knowledge only on a two-phase fibre suspension of fibres and liquid water. This means that an entirely new and exciting field of CFD simulation needs to be researched to obtain accurate results of cavitating fibre suspension flow.

8.2 Experimental work

In order to verify the results from computer simulations prototypes must be built and tested experimentally. Until verified by actual experimental work CFD simulations can only be considered guidelines, especially when previously untested simulation cases are being run, as for instance the cavitating flow with fibres.

However, this is not the only rationale for performing experimental work, it also offers the possibility to test mechanisms that are not readily modelled numerically. In this case for instance, the fibrillation and processing of fibres in the cavitation zone is quite complex to model numerically, we may only ever obtain a rather simplistic estimate for these effects numerically. Experimentally however it is possible to obtain accurate results on how the fibre degrades in the cavitation zone, and compare this to results obtained in conventional refiners.

Experimental work is expensive and labor consuming, especially for large scale prototypes, so first experimental tests need to be conducted on a laboratory scale, purely as a way of verifying the results from the CFD calculations. If results are positive and correlate well with simulations it would be relevant to continue with tests on a larger scale, as a suggestion on a pilot scale in an existing pulp and paper mill to see both how the design can be controlled on a large scale, as well as how well it performs in refining the fibre from wood.

Bibliography

- F. M. Alam, K. R. McNaught, and T. J. Ringrose. A comparison of experimental designs in the development of a neural network simulation metamodel. *Simulation Modelling Practice and Theory*, 12(7):559–578, 2004.
- ANSYS® Academic Research. Release 15.0, Help System, FLUENT Multiphase Analysis Guide, ANSYS Inc.
- L. J. Briggs. Limiting negative pressure of water. *Journal of Applied Physics*, 21(7):721–722, 1950.
- C. A. C. Coello, G. T. Pulido, and M. S. Lechuga. Handling multiple objectives with particle swarm optimization. *Evolutionary Computation, IEEE Transactions on*, 8(3):256–279, 2004.
- C. T. Crowe. *Multiphase flow handbook*. CRC Press, 2005.
- C. T. Crowe and E. E. Michaelides. Basic concepts. In C. T. Crowe, editor, *Multiphase Flow Handbook*, chapter 1, pages 1–69. CRC Press, 2005.
- C. T. Crowe, J. D. Schwarzkopf, M. Sommerfeld, and Y. Tsuji. *Multiphase Flows with Droplets and Particles*. CRC Press, second edition, 2011.
- L. Davidson. Fluid mechanics, turbulent flow and turbulence modeling. Course material, Applied Mechanics, Chalmers University of Technology, 2014.
- R. C. Eberhart and J. Kennedy. A new optimizer using particle swarm theory. In *Proceedings of the sixth international symposium on micro machine and human science*, volume 1, pages 39–43. New York, NY, 1995.
- Energimyndigheten. ET2013:22 Energiläget 2013. Government report, Statens Energimyndighet, 2013.
- O. Eriksen and L.-Å. Hammar. Refining mechanisms and development of tmp properties in a low-consistency refiner. In *Int. Mech. Pulp. Conf., Minneapolis, MN, USA*, 2007.

- European Commission. The 2020 climate and energy package, 2014. URL http://ec.europa.eu/clima/policies/package/index_en.htm.
- K.-T. Fang, R. Li, and A. Sudjianto. *Design and Modeling for Computer Experiments*. Chapman and Hall/CRC, Boca Raton, 2006. doi: 10.1201/9781420034899.
- F. D. Foresee and M. T. Hagan. Gauss-newton approximation to bayesian learning. In *Proceedings of the 1997 international joint conference on neural networks*, volume 3, pages 1930–1935. Piscataway: IEEE, 1997.
- J.-P. Franc. Physics and control of cavitation. Technical report, DTIC Document, 2006.
- J.-P. Franc and J.-M. Michel. *Fundamentals of cavitation*, volume 76. Springer, 2006.
- P. R. Gogate. Hydrodynamic cavitation for food and water processing. *Food and Bio-process Technology*, 4(6):996–1011, 2011.
- P. R. Gogate and A. B. Pandit. Hydrodynamic cavitation reactors: a state of the art review. *Reviews in Chemical Engineering*, 17(1):1–85, 2001.
- P. R. Gogate and A. B. Pandit. A review and assessment of hydrodynamic cavitation as a technology for the future. *Ultrasonics sonochemistry*, 12(1):21–27, 2005.
- M. Illikainen, E. Harkonen, M. Ullmar, and J. Niinimäki. Power consumption distribution in a tmp refiner: comparison of the first and second stages. *Tappi Journal*, 6(9): 18, 2007.
- IPCC Intergovernmental Panel on Climate Change. Climate change 2013 - the physical science basis. Technical report, IPCC, 2013.
- Ö. Johansson and L. Landström. Slutrapport: Hur kan resonansfenomen utnyttjas för att minska energiförbrukningen vid framställning av papper. Technical report, ÅForsk, 2010.
- A. Lundberg. Efficient automatic vehicle shape determination, 2014.
- F. R. Menter. Performance of popular turbulence model for attached and separated adverse pressure gradient flows. *AIAA journal*, 30(8):2066–2072, 1992.
- A. Mroziński. Modelling of waste-paper stock treatment process in disc refiners. *Journal of POLISH CIMAC*, (3):113–119, 2010.
- Naturvårdsverket. Underlag till en färdplan för ett Sverige utan klimatutsläpp 2050. Government report, Naturvårdsverket, 2012.
- T. Okada, Y. Iwai, and K. Awazu. A study of cavitation bubble collapse pressures and erosion part 1: A method for measurement of collapse pressures. *Wear*, 133(2): 219–232, 1989.

- N. Rajabi Nasab. Understanding of no-load power in low consistency refining. 2013.
- J. Sauer. *Instationär kavitierende Strömungen: ein neues Modell, basierend auf front capturing (VoF) und Blasendynamik*. PhD thesis, Karlsruhe, Univ., Diss., 2000, 2000.
- G. Schnerr and J. Sauer. Physical and numerical modeling of unsteady cavitation dynamics. In *Fourth International Conference on Multiphase Flow, New Orleans, USA*, volume 1, 2001.
- J. Selin. Tanke och handling, 2014. URL <http://hdl.handle.net/2077/35317>.
- V. Shankar. Fluid induced cavitation to improve energy efficienct in disc refiner for paper and pulp production - application of advanced research techniques. Technical report, ÅF Consulting, 2014.
- V. Shankar, A. Lundberg, K. Frenander, L. Landström, and Ö. Johansson. Design of venturi using hydrodynamic cavitation. To be published 2015.
- Statistiska centralbyrån. Industrins årliga energianvändning 2012, slutliga uppgifter. Government report, Statens Energimyndighet, 2014.
- R. A. Van den Braembussche. Numerical optimization for advanced turbomachinery design. In D. Thévenin and G. Janiga, editors, *Optimization and Computational Fluid Dynamics*, chapter 6, pages 147–191. Springer-Verlag, Berlin, 2008.
- H. K. Versteeg and W. Malalasekera. *An introduction to computational fluid dynamics: the finite volume method*. Pearson Education, 2007.
- D. C. Wilcox. Reassessment of the scale-determining equation for advanced turbulence models. *AIAA journal*, 26(11):1299–1310, 1988.